Air Force Institute of Technology

AFIT Scholar

6-1997

Residual Strength after Fatigue of a Cross-Ply Metal Matrix Composite at Elevated Temperature

Alvin N. Ruiz

Follow this and additional works at: https://scholar.afit.edu/etd

Part of the Structures and Materials Commons

Recommended Citation

Residual Strength After Fatigue of a Cross-Ply Metal Matrix Composite at Elevated Temperature

Alvin Ruiz

Captain, USA

AFIT/GAE/ENY/97J-1

DTIC QUALITY INSPECTED 2

The views expressed in this thesis are those of the author and do not reflect the official policy or position of the Department of Defense or the U.S. Government.
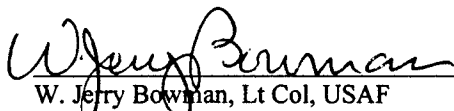
RESIDUAL STRENGTH AFTER FATIGUE OF A

CROSS-PLY METAL MATRIX COMPOSITE AT

ELEVATED TEMPERATURE
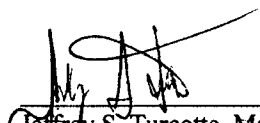
Alvin Ruiz
Captain, USA

Approved:

Dr. Shankar Mall
Professor and Head, Chairman

W. Jerry Bowman, Lt Col, USAF
Deputy Head and Associate Professor of Aerospace Engineering

Jeffrey S. Turcotte, Maj, USAF
Assistant Professor of Aeronautical Engineering

Acknowledgments

Table Of Contents

List Of Figures

List Of Tables

Abstract

The advancement of technology requires lightweight materials which exhibit good mechanical properties at elevated temperature. The stiffness and strength requirements placed on certain materials operating at high temperature can no longer be met by most traditional metals. Metal Matrix Composites (MMCs) are currently being considered as possible candidates in applications where materials with high strength and modulus, under elevated temperature, are needed. Among composite materials, MMCs are receiving a great deal of attention concerning operation under high temperature regimes.

The objective of this study was to investigate the residual strength of a cross-ply, $[0/90]_{2s}$, SCS-6/Ti-15-3, metal matrix composite (MMC) at elevated temperature (427°C) when exposed to fatigue loading. To accomplish this, several specimens were subjected to a strain-controlled, fully reversed loading (R= -1), at various strain levels. The specimens were fatigued up to a portion of their life expectancy and then loaded to failure. One specimen was also cycled to failure at 0.3% maximum strain to corroborate data obtained from previous works. Stress and strain data obtained during the test provided useful information for the macro-mechanical behavior of the material. Furthermore, the fracture surfaces and interior of specimens were examined to characterize the damage and failure mechanisms.

It was found that the residual strength degradation of the $[0/90]_{2s}$ cross-ply followed a linear relationship when plotted against a normalized percentage of their ex-

pected fatigue lives at each strain level. Furthermore, the normalized residual strength at different strain levels fell on a narrow scatter band which gradually decreased with increasing number of normalized cycles. It was determined that the residual strength was directly related to the amount of damage present in the matrix, meanwhile, the amount of matrix damage was dependent on the number of cycles and strain level the specimen had been exposed to. Matrix-fiber debonding and matrix cracking were determined to be the primary fatigue fracture mechanisms. Most of the cracks leading to specimen failure originated at the 90° and then extended towards the 0° fibers.

In comparing the current work with a previous study under load controlled mode, it was observed that the residual strength under the strain controlled mode degraded more consistently than its counterpart under load controlled mode. This variation, however, may be due to the frequency and R-ratio differences between the two loading modes since previous works have shown that the fatigue damage mechanisms of a cross-ply MMC tested under strain control will be the same as those tested under load control at the same stress ratio.

The comparison of the residual strength degradation of the cross-ply vs. unidirectional laminates reflected a significant difference due to ply orientation. The unidirectional composite exhibited much less residual strength degradation due to the absence of the crack initiation action attributed to the 90° plies in the cross-ply.

Residual Strength After Fatigue of a Cross-Ply Metal Matrix Composite at Elevated Temperature

1. Introduction

Since ancient times and the use of adobe, humans have known the usefulness of mixing different elements to obtain materials with desired characteristics. In an attempt to overcome the limiting properties of common structural metals, numerous studies have been conducted in the area of composite materials. Composites are formed by combining two or more materials to produce a combination of properties that can not be achieved by either of the constituents acting alone. A good example of a composite material is a fiber-reinforced composite which consists of fibers embedded in a matrix. The advancement of technology and the application of composite materials in the aerospace industry has created a great demand for light materials with good mechanical properties.

Among composite materials, Metal Matrix Composites (MMCs) are receiving a great deal of attention for retaining their properties under high temperature applications. MMCs are metal alloys reinforced with high strength and stiffness fibers[26] . The two most commonly used metal matrices are aluminum and titanium; of these two, the titanium has higher tensile strength-weight ratio as well as better strength retention at higher temperatures [16] . The SCS-6/Ti-15-3, also known as Titanium Metal Composite (TMC), is a MMC which has received a great deal of attention by various researchers since it is a good model material for many titanium matrix composites. It is composed of a titanium matrix reinforced with continuous silicon carbide fibers. Its

1

high strength and light weight properties along with the good thermal resistance makes it a good material which offers the potential for meeting most of the weight and strength requirements of the aerospace industry.

Several studies have been conducted to understand the fatigue behavior of the SCS-6/Ti-15-3. For example, Dennis investigated the fully-reversed fatigue behavior and damage mechanisms in a cross ply, $[0°/90°]_{2s}$, SCS-6/Ti-15-3 composite, at elevated temperature [7] . This was accomplished by using a tension-compression, strain-controlled loading mode at a strain rate of 0.2%/sec. Boyum studied the tension-compression fatigue behavior of SCS-6/Ti-15-3, with the cross-ply lay-up of $[0°/90°]_{2s}$, under load controlled mode, at room and elevated temperatures [1] . Another tension-compression fatigue study was performed by Kraabel [12] where the tests were conducted with uni-directional SCS-6/Ti-15-3, under load controlled, fully-reversed cycling, at a temperature of 427° C. The effects of volume fraction on the fatigue behavior of unidirectional TMC, under strain controlled mode at elevated temperature, was studied by Coghlan [5] . Although a significant amount of research has been conducted to study the fatigue behavior of metal matrix composites, there is still a great deal of work needed before this material can be reliably used in critical components.

An area which has received little attention, but is of particular interest in the characterization process of this material, is the study of its residual strength after exposure to fatigue loading. As the specimen is cycled, damage starts accumulating in the fibers and matrix; this damage may have a significant effect on the residual strength of the ma-

2

terial. Since the amount of damage is directly related to the test condition, the residual strength may also be affected by fatigue.

Recently, Chiou investigated the residual strength of unidirectional and cross-ply laminates of SCS-6/Ti-15-3 composite at 427°C, when subjected to fatigue loading under load control mode [4]. The present study is the continuation of his work and its purpose is to investigate the effects of various test parameters, such as R ratio and fatigue control mode, on the degradation of the residual strength of SCS-6/Ti-15-3, $[0/90]_{2s}$ cross-ply laminates when subjected to fatigue loading at a temperature of 427°C. Fatigue tests were, therefore, performed under tension-compression loading conditions, in strain control mode, with a triangular waveform. All the tests were performed at a strain rate of 0.1%/sec and R= -1. One test was cycled to failure at 0.3% maximum strain to corroborate data from a previous study, while the remaining tests were stopped at various fractions of the specimen's life expectancy and then monotonically loaded to failure to determine the residual strength. During the cycling tests, stress and strain data were monitored for understanding of fatigue behavior. After specimen failure, fracture surfaces and sectioned specimens were analyzed using optical and scanning electron microscopes to document the fatigue damage and failure mechanisms. Although several studies have been performed on load control mode and unidirectional specimens [1] [4] [12], very little work has been done on cross-ply under strain control [7]. The overall purpose of this research is to broaden the current knowledge base of the residual strength of the TMC, SCS-6/Ti-15-3 after exposure to fatigue.

2. Previous Works

Throughout this study, reference will be made to previous research performed on MMCs related to the present study. The data obtained here will be used to expand or corroborate the existing knowledge. To better understand the scope of this research, a brief background of related previous work is provided in this section.

2.1 Monotonic Tests

There have been numerous studies of MMCs under monotonic loading such as those conducted by Lerch and Saltsman [14] where laminated, continuous SiC-fiber-reinforced Ti-15-3 composites were pulled in tension to failure in order to study their damage mechanisms. These experiments were conducted at room temperature and at 427 °C. Detailed fractography and metallography were performed to identify the failure modes. Selected specimens were interrupted at various strain increments and examined to document the development of damage. Laminate orientations tested were $[0°]_8$, $[90°]_8$, $[0°/90°]_{2s}$, $[90°/0°]_{2s}$, $[\pm 30°]_{2s}$, $[\pm 45°]_{2s}$ and $[\pm 60°]_{2s}$. They found that, at room temperature, the $[0°]_8$ lay-up is the strongest, followed in order of decreasing strength by the $[0°/90°]_{2s}$, $[90°/0°]_{2s}$, $[\pm 30°]_{2s}$, $[\pm 45°]_{2s}$, $[90°]_8$, and $[\pm 60°]_{2s}$ lay-ups. They observed that specimens tested at 427 °C showed an increase in matrix ductility at this temperature as evidenced by matrix necking on the fracture surface. This behavior was not observed in specimens tested at room temperature. These specimens also

showed extensive fiber cracking and debonding near the fracture surface. The $[0°]_8$ lay-up showed little fiber-matrix debonding before failure.

2.2 Fatigue Behavior

There have been numerous studies reported involving investigation of fatigue behavior of MMCs. In the following sections a few representative studies for each loading case are discussed.

2.2.1 Tension-Tension

Portner investigated fatigue damage initiation and progression in SCS-6/Ti-15-3 at an isothermal temperature of 427 °C [23] . This investigation was conducted with a cross-ply lay-up of $[0°/90°]_{2s}$ at two frequencies, 2 Hz and 0.02 Hz. The results of this study showed the existence of the same limiting strength of 370 MPa at 50,000 cycles under all test conditions. It also segregated the failure modes of the specimens into two different groups based on the strain at failure. In the first group, 2.0 Hz, the high frequency cycling caused the matrix to become strain hardened and to fail prior to the fiber. In the second group (0.02 Hz) fiber failure preceded matrix failure with a final failure mode due to ductile void coalescence. The specimens cyclically stressed at lower loads had transverse matrix cracking initiating out of the fiber matrix interfaces more commonly than those at higher load. No evidence of ply delamination was found in any specimens.

2.2.2 Tension-Compression

The tension-compression fatigue behavior of a titanium-based, metal matrix composite reinforced with silicon carbide fibers, SCS-6/Ti-15-3, with the cross-ply lay-up

of $[0°/90°]_{2s,}$ was investigated at room temperature by Boyum and Mall [2] . The specimens were tested under tension-tension and tension-compression cycling conditions with a stress ratio of 0.1 and -1.0, respectively. They observed that the tension-compression specimens had shorter fatigue lives than the tension-tension specimens on a maximum stress basis. They attributed this to additional damage mechanisms which developed in the tension-compression cycling condition. On the other hand, in the stress-range basis they found the tension-compression fatigue life to be longer than tension-tension. This was believed to be caused by the presence of a tensile mean stress. Based on the stress-strain response and subsequent microscopic evaluations, the fatigue behavior was categorized in three distinct regimes. Those were fiber-dominated, matrix dominated, or mixed.

Another set of tension-compression fatigue test, under load controlled, fully reversed, was performed by Kraabel [12] . The tests were conducted at a temperature of 427° C. The goal of the research was to expand on previous work done by Mall and Boyum [2] . Similar to Dennis [7] , Kraabel divided the fatigue life diagram into three regions based on Talreja's fatigue life diagram [25] . Tension-tension fatigue tests were also conducted to compare with the tension-compression results. He concluded that, based on the maximum stress or strain, the fatigue life under fully-reversed, tension-compression cycling is less that for tension-tension [12] .

2.3 Fully Reversed Strain-Controlled Mode

Dennis investigated the fully-reversed fatigue behavior and damage mechanisms in a cross ply, $[0°/90°]_{2s,}$ SCS-6/Ti-15-3, at elevated temperature [7] . This was accom-

plished by using a tension-compression, strain-controlled loading mode at a strain rate of 0.2%/sec. From the results, it was concluded that damage in the longitudinal plies have the most significant effect on the fatigue response of the cross-ply laminate. He also concluded that, when compared on a strain range basis, the fatigue life of the cross-ply laminate subjected to fully-reverse loading is independent of control mode. Dennis categorized his data into three major failure modes: fiber dominated, mixed fiber and matrix, and matrix dominated. This concept of categorizing failure modes based on the predominant failure characteristics was originally studied by Talreja [25]. Dennis' data, as seen in Figure 1, provided life expectancy information for the current work. The life expectancy for the 0.4% maximum strain was 12,500 cycles, that of the 0.3% maximum strain was 22,000 cycles and the 0.25% maximum strain had a life expectancy of 70,000 cycles [7].

2.4 Hybrid Strain Controlled Mode

Sanders and Mall [24] investigated the fatigue response of an eight-ply, unidirectional, titanium-based metal matrix composite (SCS-6/Ti-15-3) at 427 °C using a hybrid strain-controlled loading mode. The results of this study were similar to the fatigue lives for the MMC tested under both load and strain controlled modes when compared on a strain-range basis.

2.5 Residual Strength

2.5.1 Load Controlled Mode

Chiou investigated the residual strength of unidirectional and cross-ply laminates of SCS-6/Ti-15-3, metal matrix composite at 427 °C, when subjected to fatigue load-
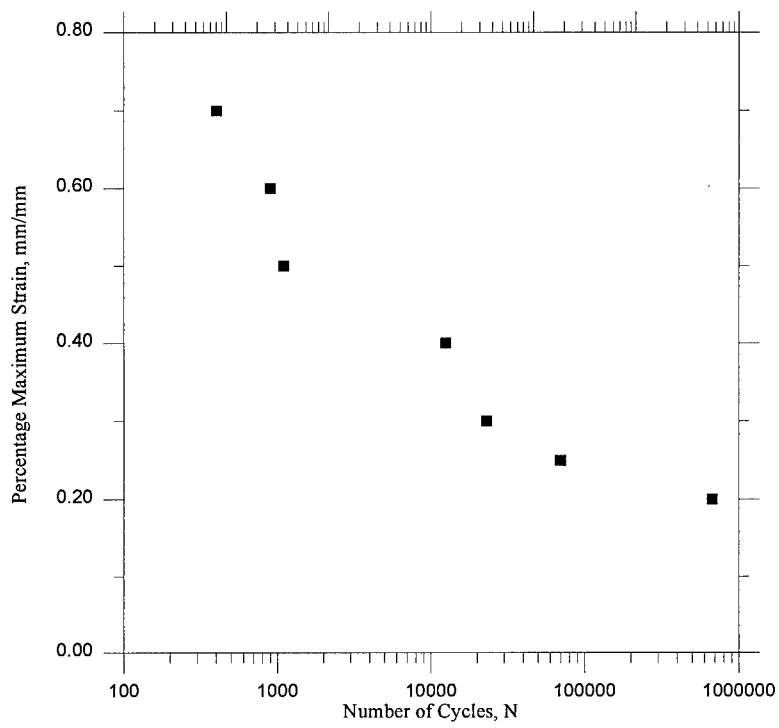
Figure 1. Percentage Maximum Strain vs. Number of Cycles [7]

ing under load control mode [4] . The purpose of his study was to determine the effects of different levels of fatigue damage on the composite's residual strength. The unidirectional specimens were cycled to 900 MPa maximum stress at a frequency of 10 Hz. The cross-ply specimens were tested at both 300 MPa and 450 MPa at 5 Hz and 10 Hz, respectively. Chiou concluded that the failure mode for the monotonic tests was dominated by the strength of the fibers for both longitudinal and cross-ply laminates.

2.5.2 Frequency Effects

In another related study, Lee investigated the residual strength, and the effects of frequency on the residual strength, for a unidirectional, SCS-6/Ti-6-4 TMC, at elevated temperature (427°C), when subjected to fatigue loading under load control mode. He observed that tests conducted at 1 Hz exhibited matrix dominated fatigue responses with a high increase in strain during the initial 10% of the life. Tests conducted at 0.01 Hz, however, showed a fiber dominated response with a faster strain rate increase [13] .

2.5.3 Fiber Fraction Effects

Coghlan [5] investigated the fatigue behavior of an unidirectional TMC laminate with three different fiber volume fractions under fully reversed, strain controlled conditions at 427°C. He concluded that the residual strength behavior of SCS-6/Ti-15-3 depends more on fiber volume fraction than the applied cyclic strain level.

Gayda and Gabb compared the isothermal fatigue behavior of unidirectional reinforced SCS6/Ti-15-3 with significantly different fiber contents [9] . The fiber contents of interest were 15, 35 and 45 volume percent. They concluded that the fatigue life of unidirectional SCS6/Ti-15-3 composite was enhanced by higher fiber content at room

temperature and at 550 °C on the stress-basis. However, strain-based comparison collapsed fatigue life for all fiber contents at 550 °C. Modest differences were observed at room temperatures. They attributed these small differences to variations in residual stress levels, fiber bridging and fiber damage. At 550 °C, matrix relaxation and environmental attack were believed to reduce the above mentioned factors.

The effects of fiber volume fraction on fatigue crack growth in unidirectional SiC/Ti-15-3 composite was also studied by Covey, Lerch and Jayaraman [6] . They studied the effect of fiber volume fraction on the fiber bridging mechanism. They observed that the fatigue crack growth behavior continued to decrease with increasing fiber volume fraction. This was attributed to the additional bridged fibers which can withstand higher applied stress and which induced crack arrest.

As seen in the previous paragraphs, there have been numerous studies conducted towards the characterization of MMCs. However, as can be observed, no previous work has been conducted to study the residual strength degradation behavior under strain-controlled fatigue. The current study attempts to broaden the current knowledge of the cross-ply laminate of SCS-6/Ti-15-3 by studying its residual strength degradation after exposure to fatigue under the strain controlled mode.

3. Material Description and Test Procedure

The purpose of this chapter is to provide a detailed description of the material and test equipment used, and the procedures followed in this research. The MMC composition and specimen geometry is described in detail along with the specimen preparation. The details of the tests procedures and equipment setup is also provided. Finally, the post-test specimen preparation and analysis are discussed.

3.1 Material Description

The material investigated in this research was a SCS-6/Ti-15-3 titanium matrix composite consisting of eight plies with an orientation of $[0/90]_{2s}$ (Figure 2). The MMC is composed of silicon-carbide fiber (SiC) and a titanium alloy matrix (Ti-15V-3Cr-3Al-3Sn wt%). The silicon-carbide fibers constitute 35% of the volume of the laminate and have a diameter of 142 microns (μm). This diameter is composed of three layers: the inner carbon core (38.4 μm) which serves as a substrate for the silicon carbide to build on, a bulk of silicon carbide which surrounds the carbon core (48.4 μm), and finally, by a complex outer shell consisting of alternating layers of silicon and carbon (3.5 μm), the outermost layer being carbon. This outer shell serves as a barrier to protect the silicon carbide from reacting with the titanium. The plates used in this study were fabricated by Textron Specialty Materials. The fiber layers, prior to being put in the matrix, are held together by woven molybdenum fibers (moly weaves). The matrix, in turn, comes as a thin cold-rolled sheet of titanium foil. The plies are assembled as desired and are

11

then heated to a temperature of about 815° C, held together under a pressure of 35 MPa. This heat and pressure combination consolidates the laminate. Some properties of the MMC constituents are shown in Table 1.

3.2 Specimen Preparation

The specimen shape chosen was a compromise between ease of use and manufacturing. Some of the specimen shapes commonly in use are rectangular, hour glass and dogbone. The selection of one over the other is mainly determined by the type of experiment and material being tested. Since our goal is to keep the specimen failure within the gage length (or middle portion of the specimen), a dogbone specimen is desirable. The dogbone specimen, however, is much more difficult to manufacture. The $[0/90]_{2s}$ lay-up, under tension-compression, will tend to fail in a plane perpendicular to the load direction and, when heated, the specimen will most likely fail within the heated zone. For those reasons a rectangular specimen was selected (Figure 3). These specimens were cut from the MMC plate using Electric-Discharge Machining (EDM) techniques.

In order to stabilize the microstructure of the matrix material , i.e. β-phase structure, the specimens were heat treated prior to testing. The procedure consisted of heating the specimens at 700° C in Argon, for a period of 24 hours. In order to minimize oxi-

Table 1. Fiber and Matrix Properties

Properties	Fiber (SCS-6)	Matrix (Ti-15-3 at RT)	Matrix (Ti-15-3 at 427°C)
Modulus (GPa)	395	90	80
Yield Strength (MPa)	-	800	525
ν	0.25	0.36	0.36

dation and to protect from impurities during the treatment, each specimen was wrapped

in Tantalum foil prior to beginning of the heat treatment process. Although heat treat-

ment can alter the microstructure of the matrix, no significant changes in the properties

of this material was observed [8] .
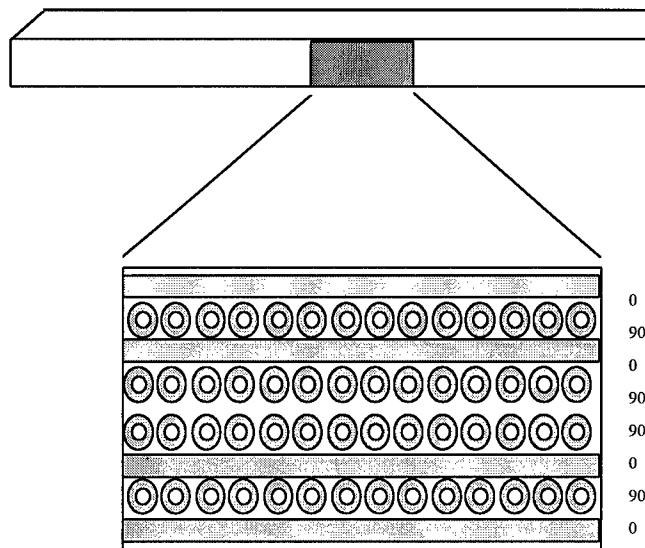
Figure 2. Cross-Ply Lay-up

3.3 Buckling Guide

Due to the thin thickness of the MMC used in this study, out-of-plane bending of

the specimens during compression was a major concern. In order to prevent this, a

buckling guide was used. This device, which is a modification of the original AFIT

buckling guide designed by Boyum[1] , is composed of four pieces (Figure 4). These

parts are held together by means of bolts and, although they fit tightly on both sides of

the specimen, the slider mechanism near the middle allows for specimen displacement.

The Guide was made of 4130 steel and was heat treated in order to harden the material.

13
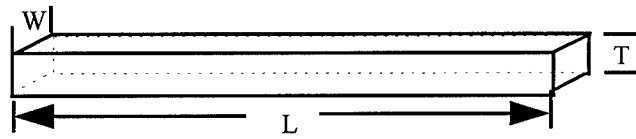
Length (L): 127 mm (5 in)

Width (W): 7.11 mm (0.28 in)

Thickness (T): 1.37 mm (0.054 in)

Figure 3. Specimens Average Dimensions
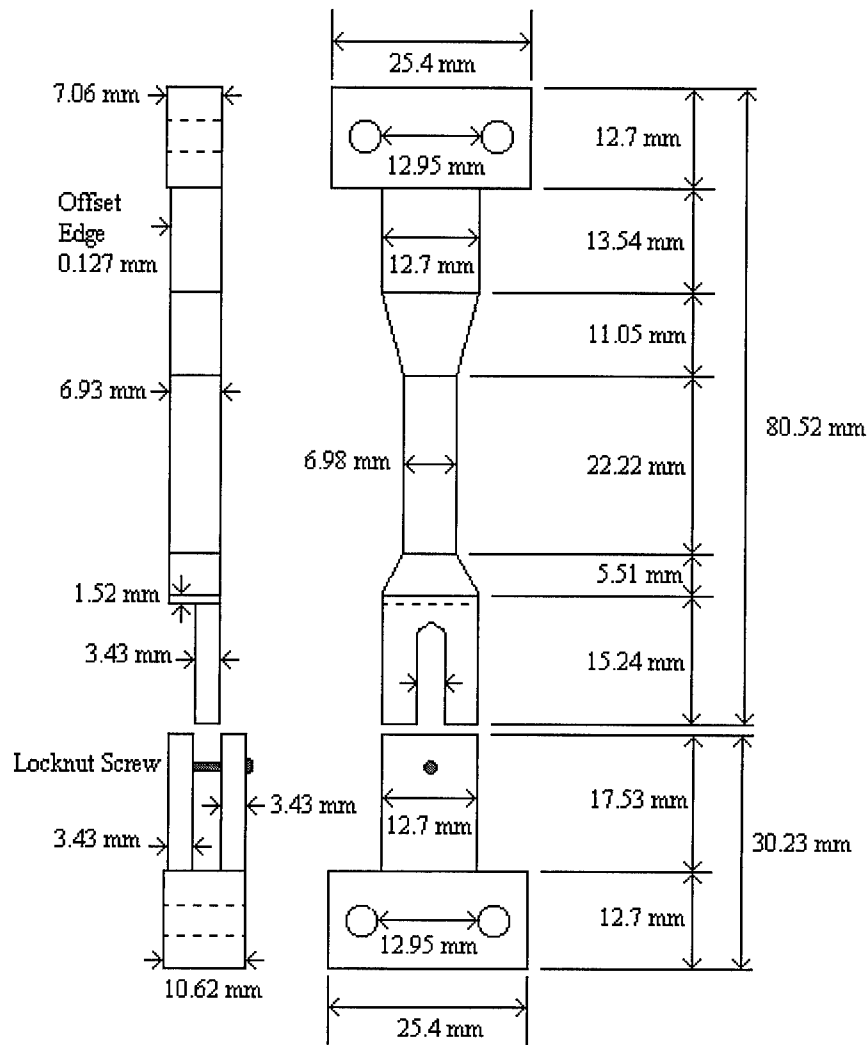
Figure 4. AFIT Buckling Guide

3.4 Test Equipment

The test equipment used in this experiment consisted of a Material Test System 808 (MTS 808), a MTS 458.20 Micro Console, and a Zenith 486 personal computer. The MTS 808 (Figure 5) is the workhorse of the three providing the actual load, or strain, to the specimen. It is a servo-mechanical screw-driven machine with a load cell of 97.8 kN (22 kip). The Micro Console controls the MTS 808 and it also allows the user to establish a safety envelope for the output of the actuator. The computer serves as the input device or, in other words, the interface between the user and the Micro Console. The software used with this computer was developed by Mark Derriso using LabVIEW from National Instruments. The computer also performs the data acquisition automatically at intervals defined by the user.

All the tests were performed at an elevated temperature of 427° C. Prior to installing the specimen on the machine, the buckling guide was installed on the specimen. The specimen was then held in the machine by hydraulic, water-cooled, friction grips at a pressure of approximately 6.9 MPa (1000 psi). To achieve the above mentioned temperature, two 1000 W, tungsten filament, water cooled, quartz lamps were located on each side of the specimen. A third lamp was placed next to the extensometer to keep it at a constant temperature distribution, correcting for changes in the ambient temperature. Both lamps heating the specimen were controlled by a Barber-Colman 560 controller, while the extensometer lamp was controlled by a Micricon controller. All lamps received temperature readings from K chromel-alumel thermocouples which were tack welded to both faces of the buckling guide or fixed to the extensometer body with alu-

16
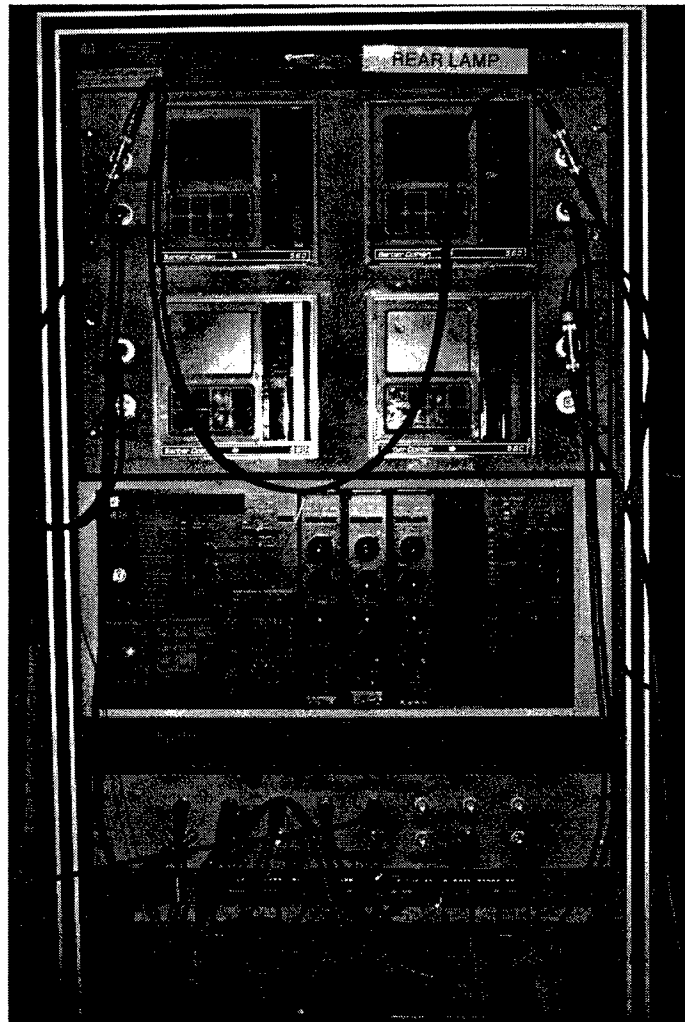
Figure 5. Material Testing System (MTS 808)

minum tape. To measure the displacement over the gauge length (12.7 mm), a ceramic rod, air-cooled extensometer (MTS model 632.50004) was used.

3.5 Test Procedures

The testing process can be broken down in the following sequential stages: specimen and equipment preparation, testing and post-failure analysis.

3.5.1 Specimen and Equipment Preparation

During this stage, the specimen's cross-sectional area is measured. The buckling guide is placed on the specimen and the latter is mounted on the bottom grips while the controller is in displacement control. A level is then used to ensure the specimen is perpendicular to the grip surface. Once proper alignment has been achieved, the lower head was moved into position. The controller was then placed on load control and the upper grips were quickly gripped onto the specimen.

Once the specimen was in position, one of the lamps was placed next to the extensometer to heat it to a temperature of 70°C. A total of twelve hours was allowed for the temperature in the extensometer to stabilize. The extensometer rods were then placed on the specimen and adjusted so that the distance between both of their tips was 12.7 mm (0.5 in) resulting in an initial strain reading of zero. The other two lamps are then placed along the specimen as close as possible to the thermocouples. At this point pertinent information such as temperature, R-ratio, data acquisition interval, etc., was entered into the computer. The specimen was then heated to 427°C and a period of 20 minutes was allowed for the temperature in the specimen to stabilize. Next the con-
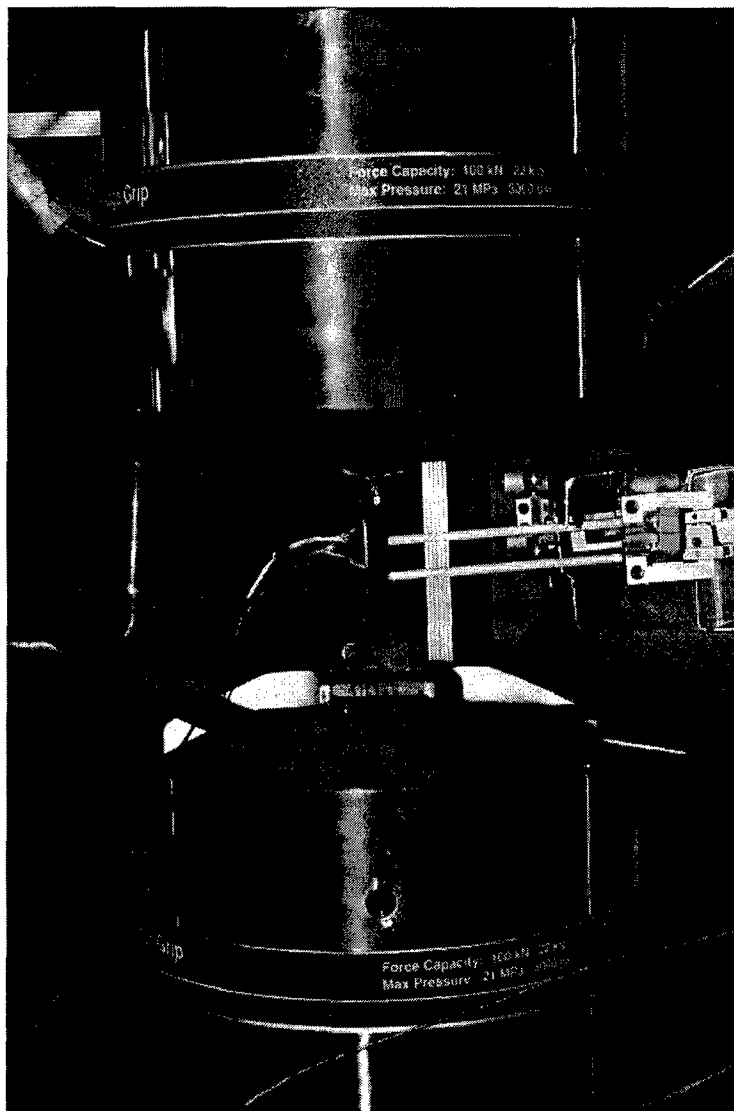
Figure 6. Specimen, Buckling Guide and Extensometer on Load Cells

troller was transferred into strain control and the safety limits enabled. At this time the span was turned up and the test started.

3.5.2 Testing

Testing takes place with very little human intervention, with the exception of mechanical difficulties such as an extensometer slippage. For residual strength testing, like that performed here, the software will stop the testing after a given number of cycles. A new set of parameters is then entered into the computer ordering the system to apply the monotonic tensile load which will bring the specimen to failure. The variables in this portion of the test procedure are the strain displacement and the percentage of the specimen's fatigue life at which the test is to be stopped. All these tests were performed under strain controlled mode, tension-compression (R= -1), triangular wave form, at maximum strains of 0.25%, 0.3% and 0.4% respectively. The strain rate was 0.1% per second. The 0.25% strain specimens were fatigue tested to 50% and 25% of their predicted life. The 0.3% strain specimens were fatigue tested to 75%, 35%, 23% and 12% their predicted life. The 0.4% strain specimens were fatigue tested to 75%, 50% and 25% of their predicted life. They were all then monotonically pulled to failure to determine the residual strength.

3.5.3 Post Failure Analysis

To prepare the specimen for post failure analysis, three small pieces were cut out of the specimen near the fracture surface (Figure 7). These pieces were cut using a low speed diamond wafering saw. Sections I and II fractured surfaces were analyzed under the Scanning Electron Microscope (SEM) and Section III was mounted, polished

20

and observed under the Optical Microscope. The following section provides a brief description of the mounting, polishing and surface analysis.
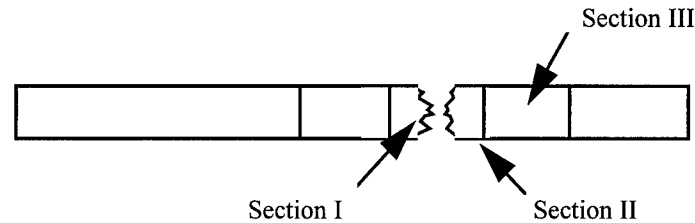
Figure 7. Fracture Specimen Sections

3.5.3.1 Mounting

Prior to observation of the fibers and matrix under the optical microscope, the specimens were polished. To facilitate the polishing, the specimens were mounted in a 25.4 mm (1 in) diameter mount using a Simplimet 2000 pressmount. The mount came in the form of a conductive phenolic mounting compound called Buehler Konductomet II. The specimen was placed on top of the ramp and then lowered to a distance of 38.1 mm (1.5 in). The powder was them poured into the chamber until the entire volume was filled. The chamber was then closed and the cycle started under a pressure of 289.57 MPa (42,000 psi). and a temperature of 150°C. The total heating time was 7 minutes, and the cool down time was 3 minutes.

3.5.3.2 Polishing

The first step is the rough polishing of the specimens using a 45μ diamond suspension on a Buehler Ultra-Plan Mesh. The force applied for this stage was 3.62 Kg (8 lbs) for about 4 min. Next, using an Ultra-Pad cloth, the specimens are further polished us-

21

ing a 15μ diamond suspension for about 8 min., at 52.26 Kg (5 lbs) force. The next step consisted of a 3μ diamond suspension on a TEXMET 1000 cloth under a 2.26 Kg (5 lbs) force for a period of approximate 4 min. The final step was on a Microcloth cloth using a chemical called Mastermet which removes all scratches larger than 0.06μ. The force applied on this step was also 2.26 Kg (5 lbs). The RPM through the polishing procedure is 150. The time required for each stage is approximate since it may vary depending on the specimen. Extreme caution was used during the first two steps since serious damage could have been done to the specimen due to the harshness of the polishing surface and the diamond suspension.

3.5.4 Surface Analysis

Upon completion of the polishing, the specimens were examined using the optical microscope and the Leica S430 SEM for micro-mechanical examination. Photographs of areas of interest were taken.

4. Results

The purpose of this chapter is to discuss the experimental results of the tests conducted during this research. Three sets of specimens, at three maximum strain levels of 0.25%, 0.3% and 0.4%, were fatigued to a certain fraction of their fatigue lives and then tested under monotonic loading for their residual strength. The expected fatigue lives were based on a previous study conducted by Dennis [7] as previously mentioned in Chapter 2. Two specimens were tested at a maximum strain of 0.25%; one fatigued to 75% and the other to 50% of their predicted life. Upon running the residual strength tests at 0.3% maximum strain value, it was realized that the estimated fatigue life at 0.3% maximum strain value from the previous study [7] was probably on the lower side, that is, the number of cycles was not high enough. Therefore, a fatigue test was conducted until failure in this study at 0.3% maximum strain. This test provided 72,700 cycles instead of the 22,000 cycles of the previous study conducted by Dennis [7] . These values were averaged and a new expected life of 47,100 was obtained for the 0.3% maximum strain. Four tests were conducted at 0.3% maximum strain which were fatigued to 75%, 35%, 23% and 12% of their predicted life based on this average value. The final set consisted of three specimens which were tested at a maximum strain of 0.4% and fatigued to 75%, 50% and 25% of their predicted life. Table 2 provides the test summary of this study. Upon completion of the fatigue portion of the experiment, all the specimens were monotonically loaded to failure and their respective residual strengths were recorded. Macro-mechanical behavior was investigated and microscopic examinations

of damaged and failure mechanisms were performed on each specimen. These results are documented in this chapter.

4.1 Macro-mechanical Evaluation

4.1.1 0.4% Maximum Strain

Three tests were conducted at this strain level, and the number of cycles to which they were fatigued were based on a life expectancy of 12,500 cycles. This value was obtained from the previous work conducted by Dennis [7]. The compression and tensile moduli for these tests were plotted separately since their behaviors were different from each other and provided insight of the damage which occurred in the specimen. These moduli were calculated from a linear fit of the compressive and tensile regions of the stress-strain curve.

The moduli vs. cycles response for the 75% expected life test is illustrated in Figure 8. After the first cycle, a considerable drop in modulus can be observed in both the compressive and tensile curves. This drop was due to fiber-matrix interface debonding of the 90°plies [11]. Thereafter, for the first 1000 cycles the compressive modulus reflects an increase of approximately 12% from 131 GPa to a 146 GPa. It then levels off until cycle 9000 (i.e. near the end of the test); this is indicative of no significant damage taking place in the matrix for approximately 8000 cycles. The increase in compressive modulus can be attributed to matrix strain hardening, or some sort of embrittlement, occurring due to exposure to high temperature. After cycle 9000, a gradual decrease is observed in both the tensile and compressive moduli suggesting that the specimen was getting very close to the end of its fatigue life. This conclusion is substantiated by

Table 2. Test Results Summary

Max Strain (mm/mm)	% of Fatigue Life	Number of Cycles	Initial Comp. Modulus (GPa)*	Final Comp. Modulus (GPa)*	Initial Tensile Modulus (GPa)*	Final Tensile Modulus (GPa)*	Monotonic Tensile Modulus (GPa)**	Residual Strength (MPa)
0.25%	50	35,000	119	141	122	123	116	647
"	75	52,500	136	146	123	119	113	524
0.3%	12	5,510	125	148	121	126	118	865
"	23	11,000	135	149	122	117	116	852
"	35	16,485	141	146	126	122	114	736
"	75	35,325	113	127	103	99	100	609
0.4%	25	3,125	124	141	113	117	107	761
"	50	6,250	147	155	120	105	102	670
"	75	9,375	136	144	127	121	101	510
* From Cyclic Stress-Strain Data								
** From Monotonic Test Slope								

observing the slope of the monotonic test for residual strength as shown in Figure 9, which shows a significant knee at about 85 MPa with a drop in initial tensile modulus from 123 GPa to about 101 GPa after the knee. This drastic reduction in the tensile modulus, at such a low stress, indicates the beginning of a catastrophic failure.

During this test, the tensile modulus decreased initially about 8% from 128 GPa to approximately 118 GPa and then increased gradually but steadily until cycle 7000. It then gradually dropped for the remainder of the test. This drop in the tensile modulus was due to damage accumulation in the specimen. As matrix damage occurred, the resistance in reaching the prescribed strain level decreased during the tensile portion of the cycling. Although the microscopic examination will later show several fiber cracks in the specimen, it is important to mention that modulus degradation is usually attributed to matrix cracking unless the gap resulting from the fiber crack is on the order of a few fiber diameters [20] .

The minimum stress curve, shown in Figure 10, displays a sudden initial magnitude increase which corresponds to the initial increase in the compressive modulus discussed earlier. It then remained constant for the rest of the test as expected. The maximum stress, on the other hand, leveled off shortly after the initial drop and it remained that way for the remainder of the test.

Figure 11 shows the stress vs. strain curves for this test. On this, and all subsequent stress-strain curve plots, the maximum and minimum strain on cycle 1 are slightly less than that desired. The reason behind this discrepancy lies on the controlling software, LabVIEW, which takes approximately 13 cycles to correct the strain value. As it can be
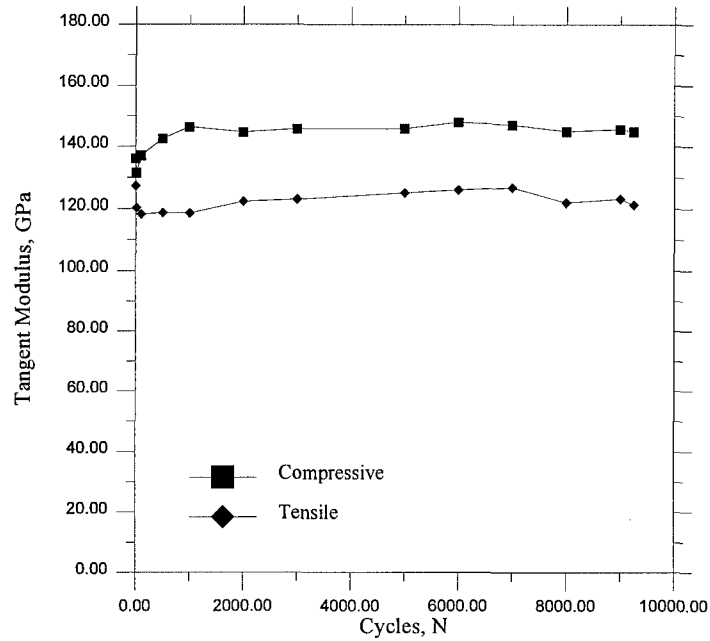
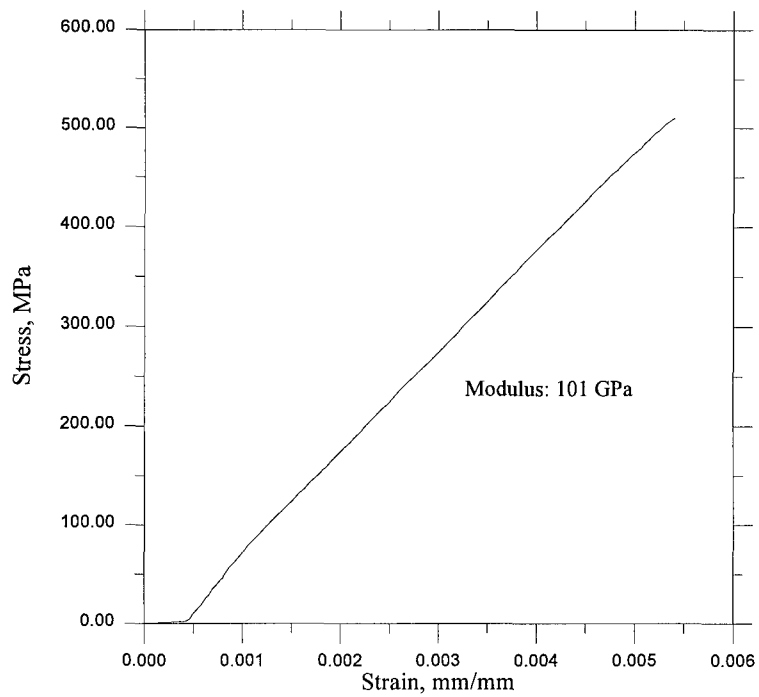Figure 8. Tensile and Compressive Modulus, 0.4% Maximum Strain, 75% Expected Life

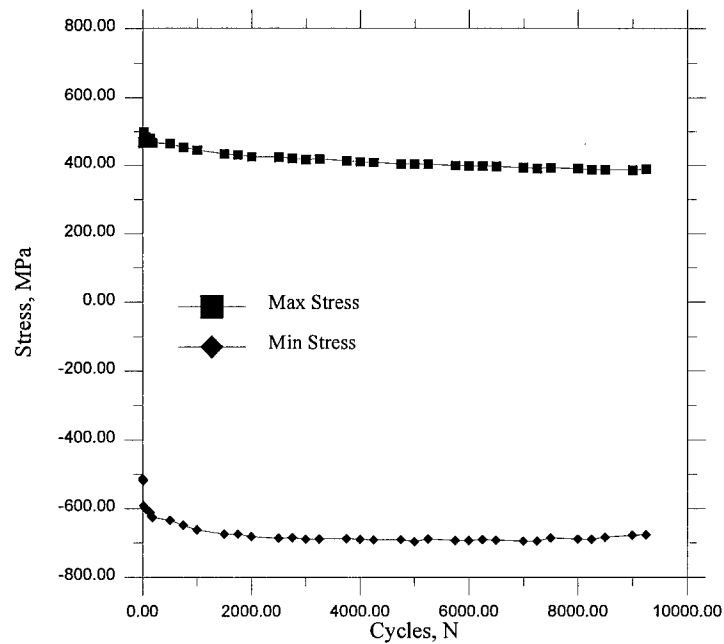Figure 9. Monotonic Test Failure, 0.4% Maximum Strain, 75% Expected Life

27

Figure 10. Maximum and Minimum Stress, 0.4% Maximum Strain, 75% Expected Life

seen in this figure, the first cycle reflects a knee at about 0.001 mm/mm corresponding to about 160 MPa. This initial stiffness drop will also be observed on follow-on tests and is attributed to the fiber-matrix interface debonding discussed earlier. Furthermore, we observe a slight residual strain present upon unloading the specimen, suggesting a slight inelastic deformation in the matrix. Had the fiber-matrix interface debonding been the only damage mechanism present, the stress-strain loop would have returned to its starting point upon unloading [15] . Subsequent cycles show a small but constant hysteresis implying that, as matrix damage accumulated, more load was transferred to the fibers which maintained the overall elastic behavior of the specimen. This matrix damage could be due to any of the following mechanism: creep, plasticity, cracking, matrix-fiber debonding, or a combination of these. Cycles 4000 and 9250 show a significant knee during the tensile portion of the cycle reflecting the drop in stiffness or modulus. Cycles 4000 and 9250 fell almost on top of each other suggesting that most of the significant damage in the matrix had taken place by cycle 4000. The residual strength for this specimen was 510 MPa with a 12.17% drop in modulus.

Initially, the 50% expected life test shows a rapid increase in compressive modulus from 139 to 147 GPa, as shown in Figure 12. Immediately after the increase, the initial drop in compressive modulus due to fiber-matrix debonding can be observed. The compressive modulus then increases gradually to about 158 GPa, at cycle 2000, and then it remained constant until the end of the test.

As seen in Figure 12, the tensile modulus shows a sudden initial drop from 120 to about 114 GPa and then a very gradual decline to 105 GPa. The final tensile modulus
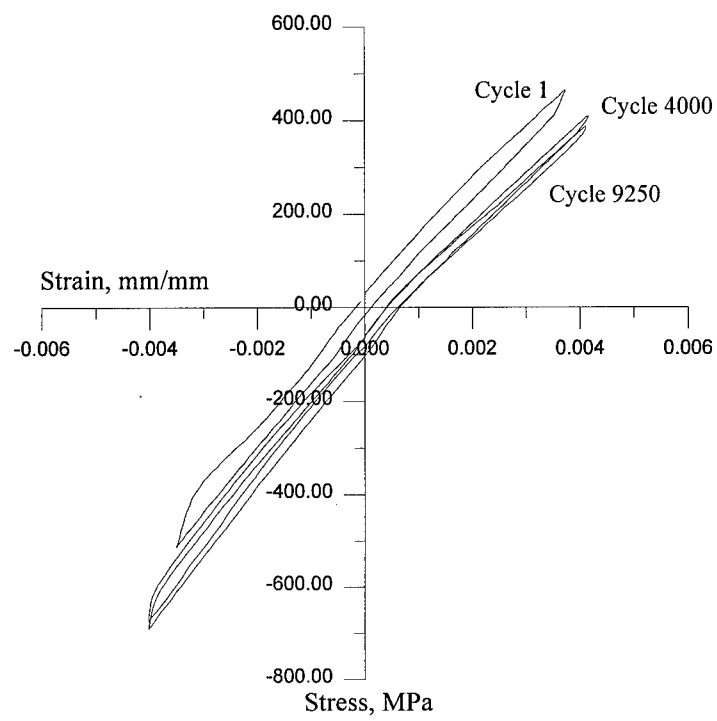
Figure 11. Stress vs. Strain Curves, 0.4% Maximum Strain, 75% Expected Life

obtained from the slope of the monotonic test was 102 GPa, which is very close to the 105 GPa obtained in the last fatigue cycle. However, on the previous test these two values were not as close. The difference lies in the fact that the current test was not as close to the end of its cyclic life as its predecessor when the tests were stopped. The slope of the monotonic test for the previous test reflected a drastic knee at about 85 MPa, on the current test, however, only a slight knee is observed and it takes place at about 450 MPa. The stress-strain curve under monotonic load for the current test is seen in Figure 58 in Appendix A.
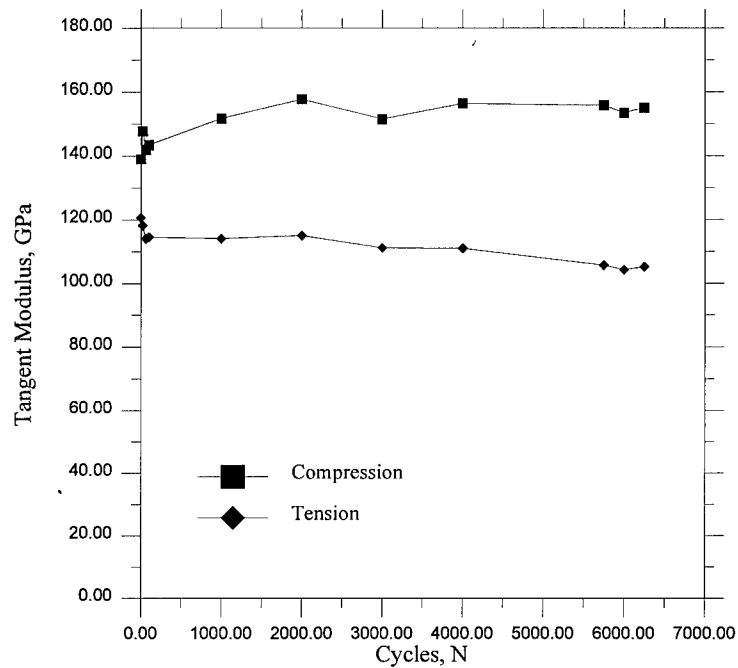
Figure 12. Tensile and Compressive Modulus, 0.4% Maximum Strain, 50% Expected Life

Both the maximum and minimum stress curves exhibit a significant change during the first cycle. As mentioned earlier, this was due to LabVIEW's adjusting period. The subsequent and more gradual change which followed both curves was the result of mod-

31
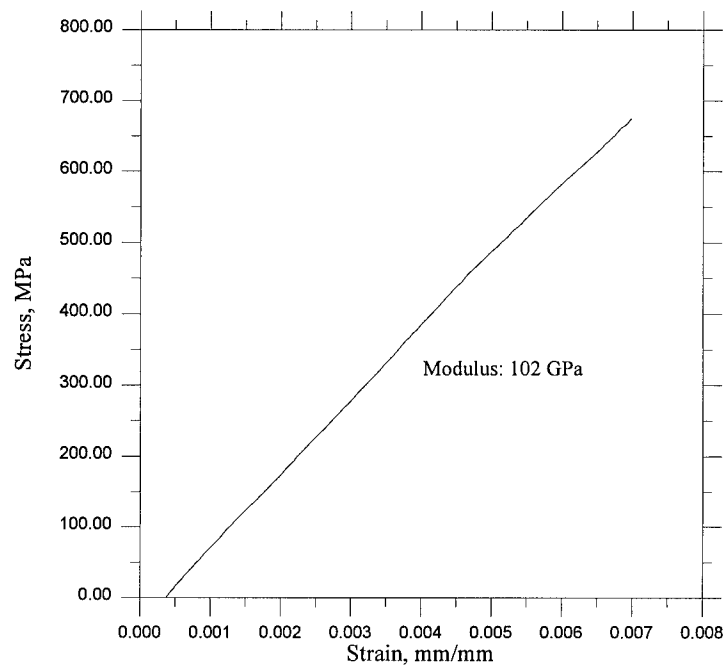
Figure 13. Monotonic Test to Failure, 0.4% Maximum Strain, 50% Expected Life

ulus change. As seen in Figure 14, the minimum stress reflects a magnitude increase

for the first 2000 cycles and then levels off at approximately -663 MPa. The maximum

stress, on the other hand, increased from 441 MPa to approximately 484 MPa and then

gradually decreased to 396 GPa.
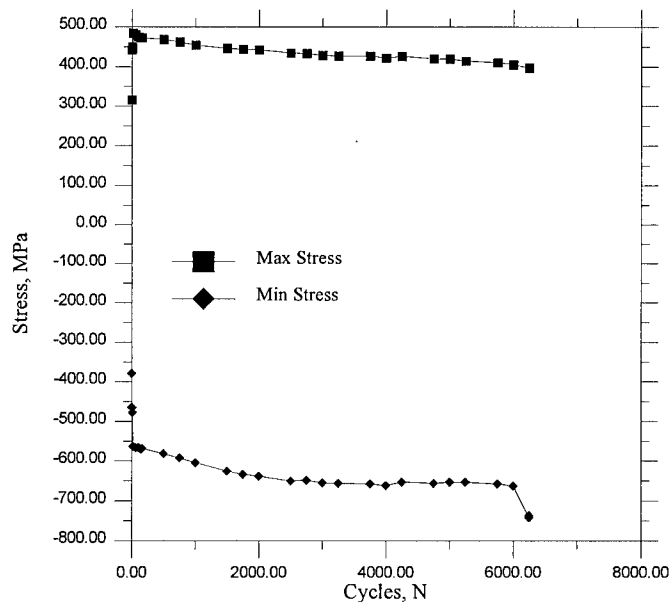
Figure 14. Maximum and Minimum Stress, 0.4% Maximum Strain, 50% Expected Life

The stress and strain curves of cycles 1, 3250 and 6250, shown in Figure 15, present

similar hysteresis curves as in the previous test. Some strain rachetting is seen on this

plot and, based on the gaps between the curves, we can conclude that most of the damage

accumulated during the first half of the test. The width observed during the tension

portion of both loops may be attributed to time dependent deformation of the matrix.

The residual strength for this specimen was 670 MPa with a 14.28% drop in modulus.

The compressive modulus increased from 124 GPa to about 141 GPa. The tensile

modulus increased slightly at a gradual rate as seen in Figure 16. The maximum and
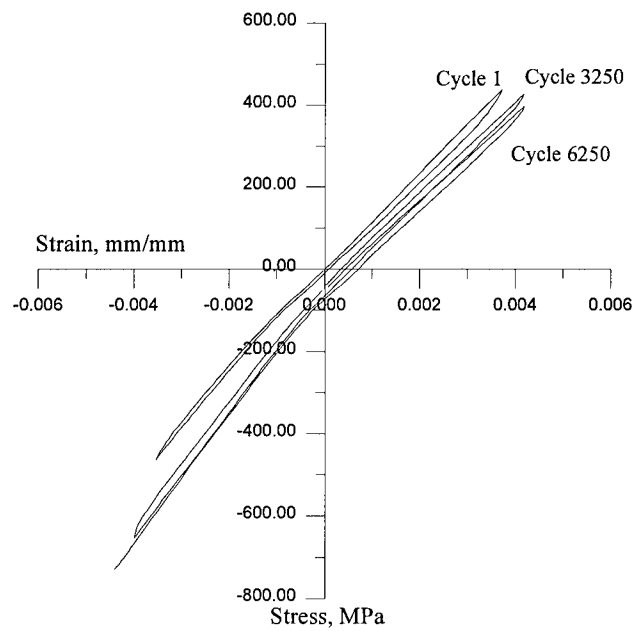
Figure 15. Stress vs. Strain Curves, 0.4% Maximun Strain, 50% Expected Life

minimum stress plot for the 0.4% maximum strain, 25% expected life test, Figure 17, reflects abnormal behavior during the first 500 cycles which was due to a gradual slip of the extensometer. At cycle 500 the test was stopped by the safety limits in the controller and then re-started after re-setting the extensometer. During this process, the specimen experienced a compression overload of approximately 120 lbs. Subsequent behavior of the material showed no signs of unusual matrix plasticity; microscopic evaluation revealed no radial cracking on the any of the fibers. These two observations indicate that no permanent damage took place on the composite while subjected to compression [18] . The data after cycle 500 follows the expected trend as displayed by previous tests.
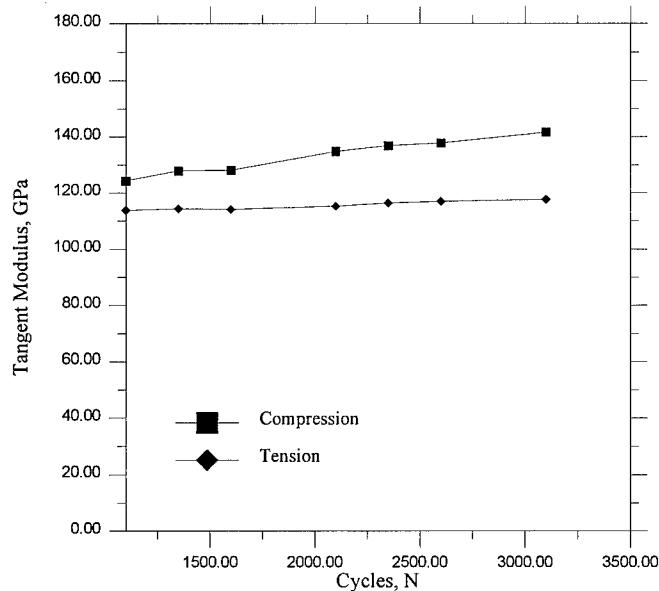
Figure 16. Tensile and Compressive Modulus, 0.4% Maximun Strain, 25% Expected Life

Following the test re-start, as mentioned earlier, the stress behavior reflects a gradual decrease in the maximum and minimum stress throughout the life of the specimen

35

as seen in Figure 17. The maximum stress changes from 481 to 426 MPa and the minimum stress from -475 to -689 MPa. Figure 17 shows the stress behavior of this test. In Figure 18, the stress and strain curves of cycles 1, 1350 and 3100 reflect a large width in the stress/strain loop of the first cycle but, upon unloading it returns to the original starting point suggesting a time dependent deformation of the matrix. The remaining cycles reflected narrower loops and overall, little strain rachetting. The residual strength was 761 MPa with a 7.75% reduction in modulus.
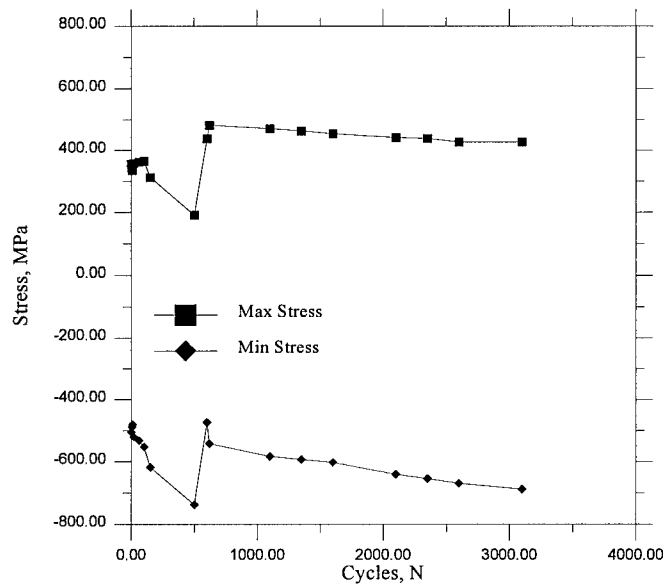
Figure 17. Maximum and Minimum Stress, 0.4% Maximum Strain, 25% Expected Life

4.1.2 0.3% Maximum Strain

The life expectancy for these tests (i.e. conducted at 0.3% maximum strain), was 47,100 cycles as mentioned previously. Figure 19 shows the modulus behavior of the 75% expected life test. Following the initial drop as seen in previous tests, the compressive modulus increases from 113 GPa to 135 GPa during a period of 6,260 cycles.
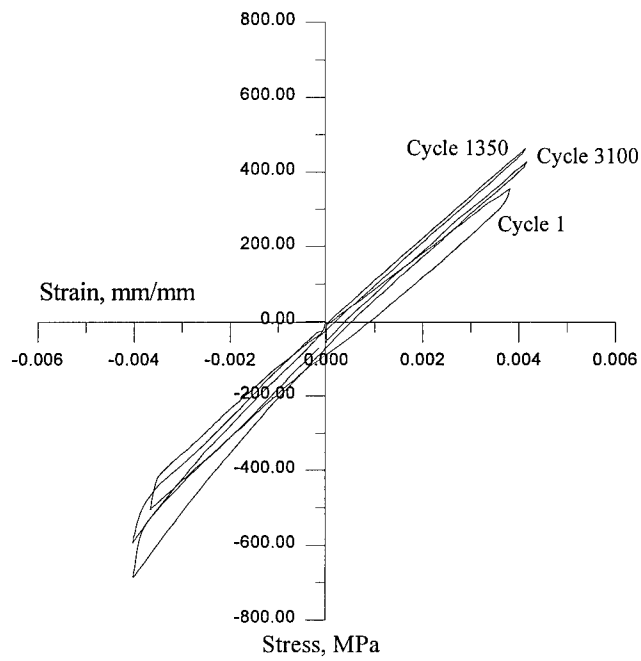
Figure 18. Stress vs. Strain Curves, 4% Maximum Strain, 25% Expected Life

This increase is similar to that experienced by its predecessor during the first 2000 cycles. Following this increase, a steady but gradual decrease was observed until the end of the test, where the compressive modulus was 127 GPa. The tensile modulus, in turn, increases from 103 to 115 GPa and then drops to 98 GPa at the end of the test.
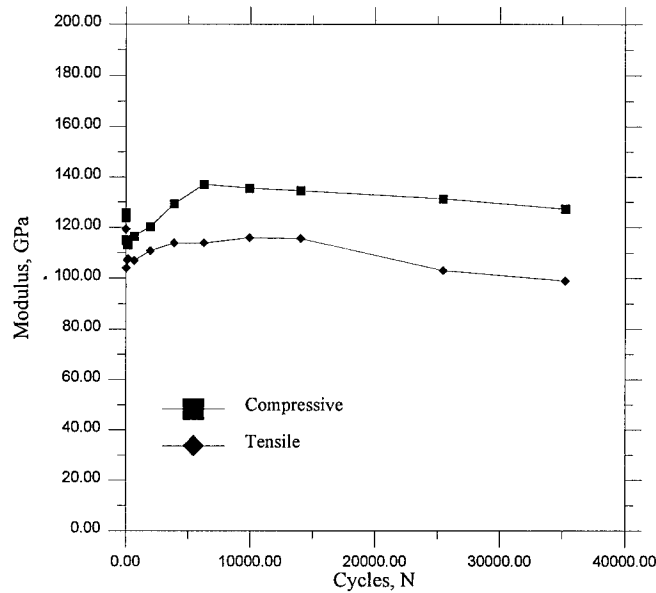
Figure 19. Tensile and Compressive Modulus, 0.3% Maximum Strain, 75% Expected Life

As can be seen in Figure 20, the maximum stress shows a steady decrease coupled with a similar decrease in the compressive stress. In addition to previous effects, this behavior can be attributed primarily to plastic deformation, or stress relaxation of the matrix. The maximum stress ranged from 341 to 252 MPa. As the specimen damage increased during the test, the maximum stress continued to decrease while the magnitude of the compressive stress increased at an equivalent rate. The minimum stress ranged from -437 to -318 MPa.

38
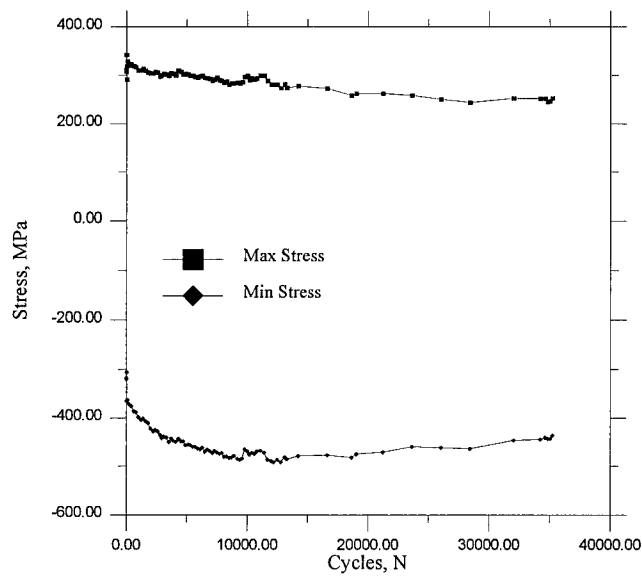
Figure 20. Maximum and Minimum Stress, 0.3% Maximum Stress, 75% Expected Life

A representation of the stress-strain response during this test is shown in Figure 21. The narrow widths of the stress-strain loops imply an almost elastic response of the matrix. This plot also shows significant strain rachetting up to cycle 35240. From this point until the end of the test very little rachetting took place. The residual strength for this test was 609 GPa with a 5% drop in modulus.
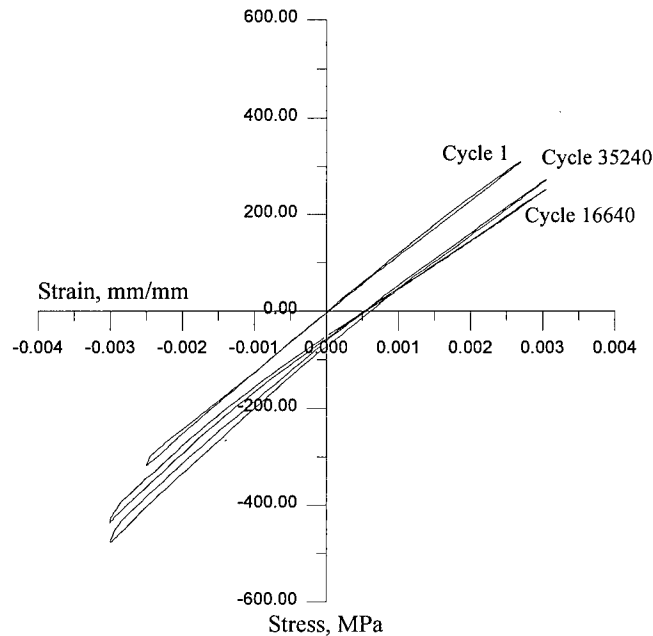
Figure 21. Stress vs. Strain Curves, 0.3% Maximum Strain, 75% Expected Life

The modulus vs. cycles response for the 35% fatigue life specimen is illustrated in Figure 22. The initial modulus for this specimen was higher than in the previous test, however, the overall behavior of the tensile and compressive moduli was very similar. The maximum and minimum stress behavior are shown in Figure 23, and it was almost identical to its predecessor. Figure 24 shows the stress vs. strain response over the duration of the test. The first cycle reflects a small change in slope at about 0.0005

40

strain in the tension portion of the loop due to the initial damage of the material. An interesting feature seen on cycle 1 is the fact that the initial unloading modulus of the cycle was greater than the initial loading modulus. Pollock and Johnson predicted this initial unloading modulus behavior using the AGLPLY program [22] . The residual strength for this specimen was 736 MPa with a 6.5% overall drop in modulus.
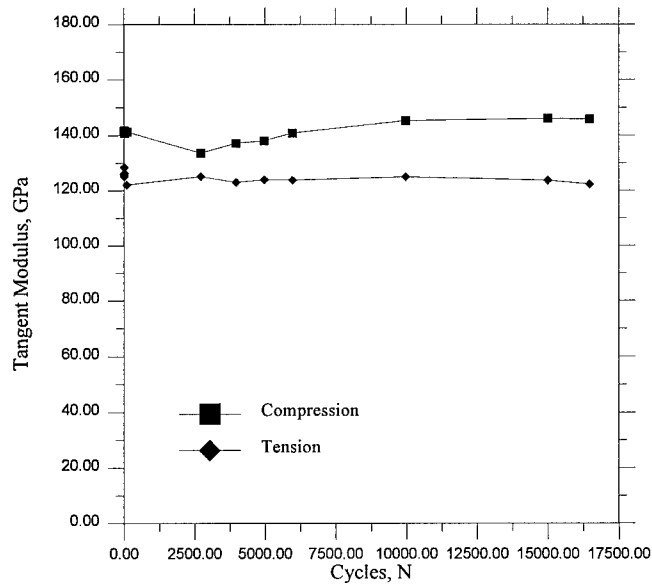
Figure 22. Tensile and Compressive Tangent Modulus, 0.3% Maximum Strain, 35% Expected Life

No differences worth noting were observed between the 23% life test and the previous tests. The initial tensile modulus was 122 GPa and the final modulus was 116 GPa equivalent to a 4.9% overall drop. The compressive modulus ranged from 135 to 149 GPa. The maximum stress ranged between 351 and 295 MPa and the minimum stress between -376 and -512 as seen in Figure 25.

The stress and strain curves of cycles 1, 6000 and 10750, depicted in Figure 26, reflect very little strain rachetting between the last two cycles. In the first cycle, the

41

Figure 23. Maximun and Minimun Stress, 0.3% Maximum Strain, 35% Expected LifeLife
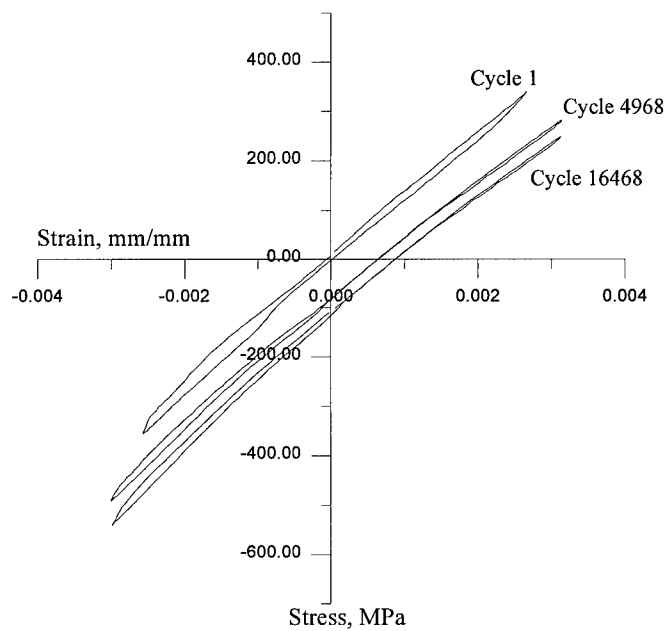
Figure 24. Stress vs. Strain Curves, 0.3% Maximum Strain, 35% Expected Life
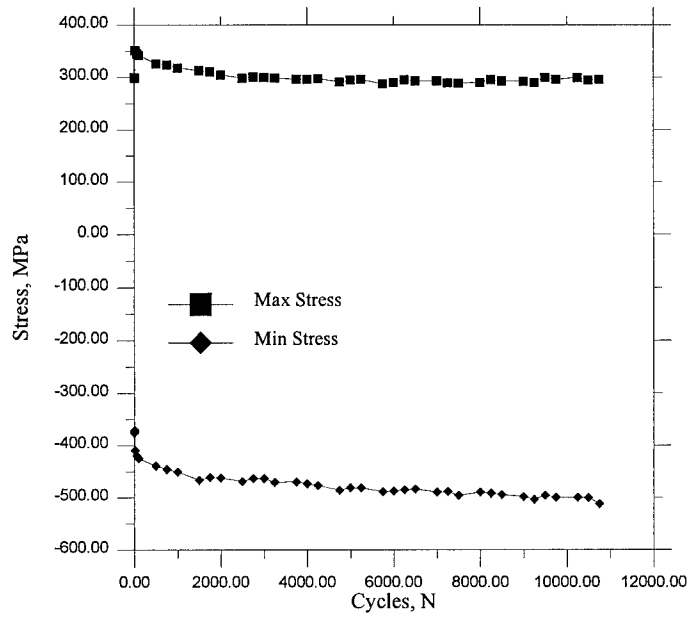
Figure 25. Maximum vs. Minimum Stress, 0.3% Maximum Strain, 23% Expected Life

unloading curve closely followed the loading curve, which implies that the separation created by failure in the fiber/matrix interface, in the off-axis plies, were closing during unloading. This is attributed to residual thermal stresses due to the significant difference in the coefficient of thermal expansion between the fiber and the matrix. The matrix has a larger coefficient than the fibers and, as the composite is cooled from the processing temperature, large compressive radial stresses build up in the interface between the matrix and the fiber [11] [17] . The residual strength was 852 MPa.
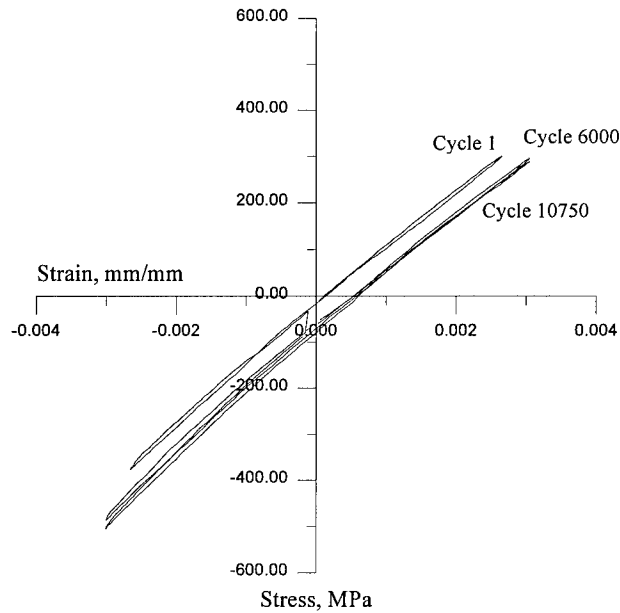
Figure 26. Stress vs. Strain Curves, 0.3% Maximum Strain, 23% Expected Life

The last test of the 0.3% maximum strain group was the 12% expected life. The compressive modulus increases from 125 GPa to about 148 GPa similar to the 23% expected life specimen, however, the increase was not as linear as its predecessor. The tensile modulus, unlike the 23% expected life, increased steadily from 121 GPa to approximately 125 GPa. The modulus curves are shown in Figure 27. The stress behavior

44

reflects a gradual decrease in the maximum and minimum stress throughout the life of

the specimen as seen in Figure 28.
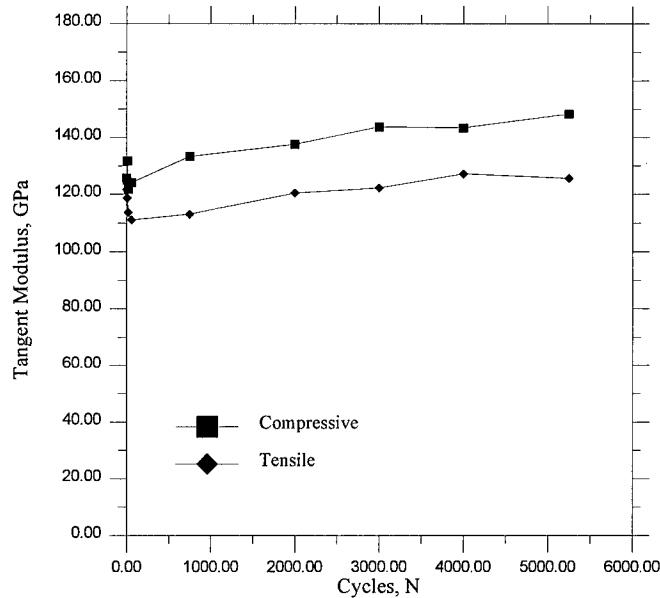
Figure 27. Tensile and Compressive Modulus, 0.3% Maximum Strain, 12% Expected Life

The stress and strain curves of cycles 1, 3250 and 5000 are shown on Figure 29.

Besides the initial damage in the specimen during the first few cycles, no more signif-

icant damage was observed on this specimen during the latter part of the test which is

reflected by the similarity between the last two stress-strain loops. In the initial loop,

the strain was fully recovered on unloading and the composite behaved essentially as

a linear-elastic solid. The stress strain response during unloading at cycle one returned

to almost a zero value of strain at a zero stress value indicating that fiber-matrix inter-

face damage was the only mechanism inducing a nonlinear response [15] . The residual

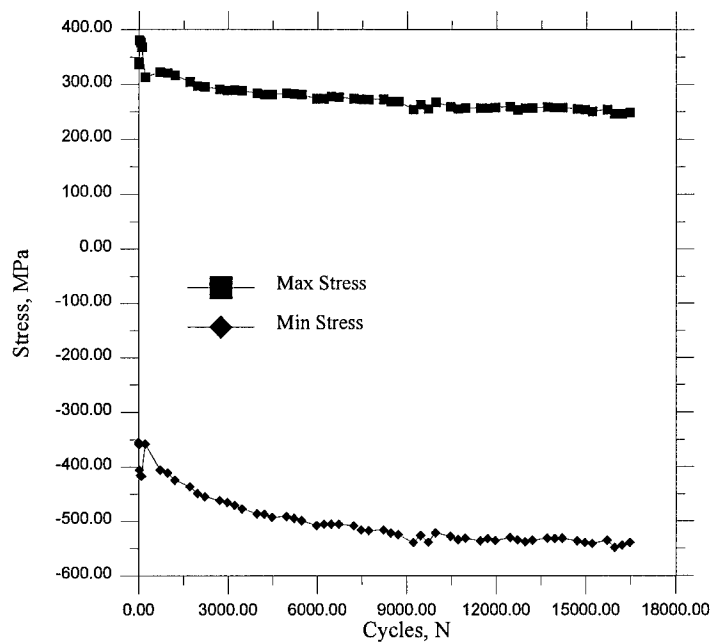strength was 856 MPa with a 8.54% drop in modulus.

45

Figure 28. Maximum and Minimum Stress, 0.3% Maximum Strain, 12% Expected Life
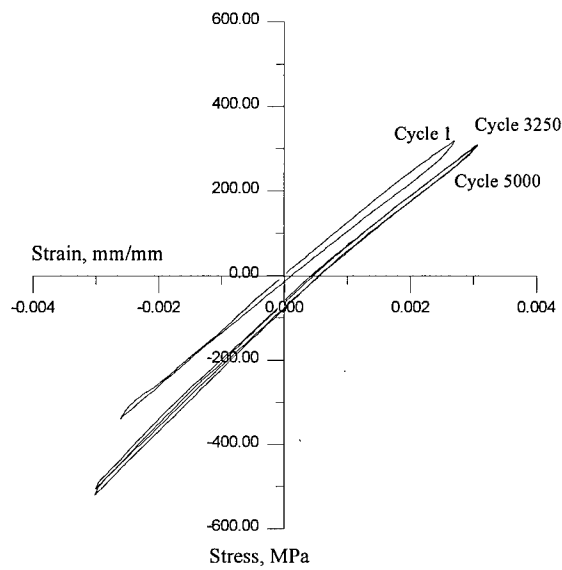
Figure 29. Stress vs. Strain Curves, 0.3% Maximum Strain, 12% Expected Life

46

4.1.3 0.25% Maximum Strain

Two specimens were tested at this strain level. The 50% expected life test was stopped at about 27,000 cycles to re-position the buckling guide; the test was then re-started. The modulus behavior seen in Figure 30 is very similar to previous tests, however, the initial knee normally seen in other tests is not obvious on this one. This may be attributed to limited debonding of fiber-matrix interfaces in the 90° fibers compared to other tests of higher maximum strain levels. The stress behavior shown in Figure 31 is also similar to previous tests with the exception of the sudden drop near cycle 27,000 due to an extensometer slippage. Looking at the stress vs. strain curves on Figure 32 we can also see that the cycle one loop starts at the zero stress/strain point, increases linearly and, during unloading, returns to the same starting point in the same linear fashion. Comparing the strain rachetting of this, and all previous tests, we observed an increase in rachetting with decreasing maximum strain level. The reason for this behavior may lie in the predominant damage mechanism present. A specimen tested at a low maximum strain, such as this one, will experience and almost entirely matrix damage mechanism while its counterpart, at 0.4% maximum strain, may have a combination of matrix and fiber damage.

4.2 Microscopic Evaluation

The purpose of this section is to study the damage mechanisms exhibited in the coupons using observations from a Scanning Electron Microscope (SEM) and to correlate them to the mechanical response for the various loading histories. Emphasis will be placed on damage initiation and propagation. The maximum strain on these tests ranged

47

Figure 30. Tensile and Compressive Modulus, 0.25% Maximum Strain, 50% Expected Life
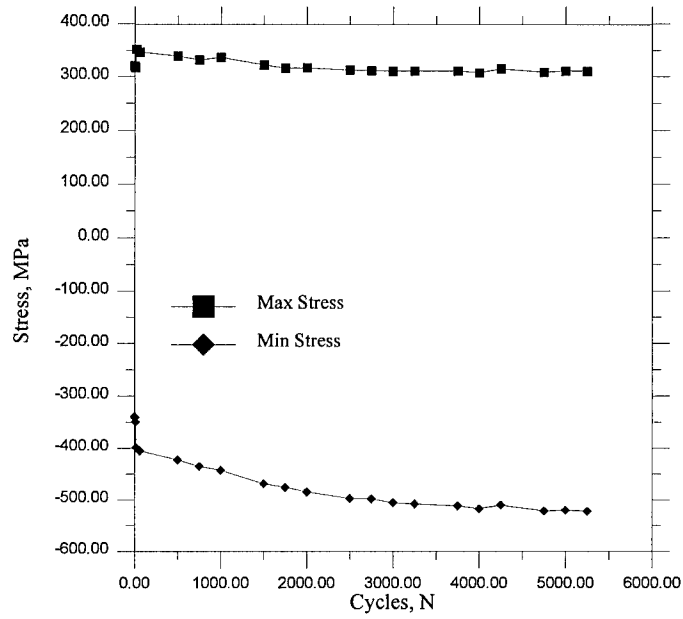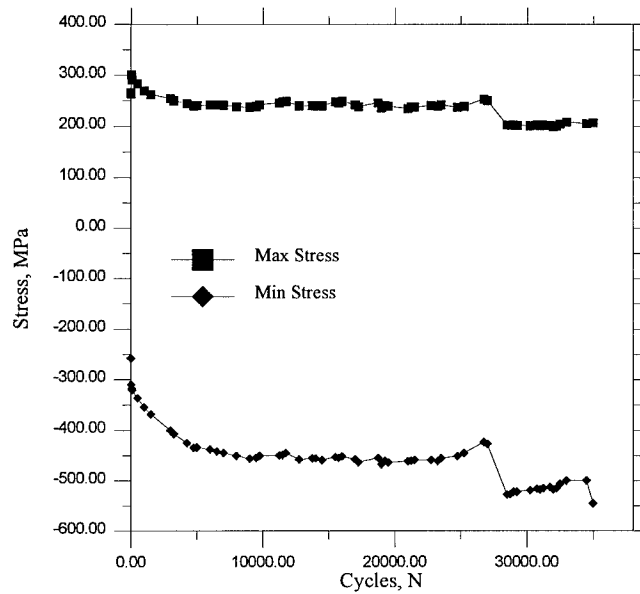

Figure 31. Maximum and Minimum Stress, 0.25% Maximum Strain, 50% Expected Life

48
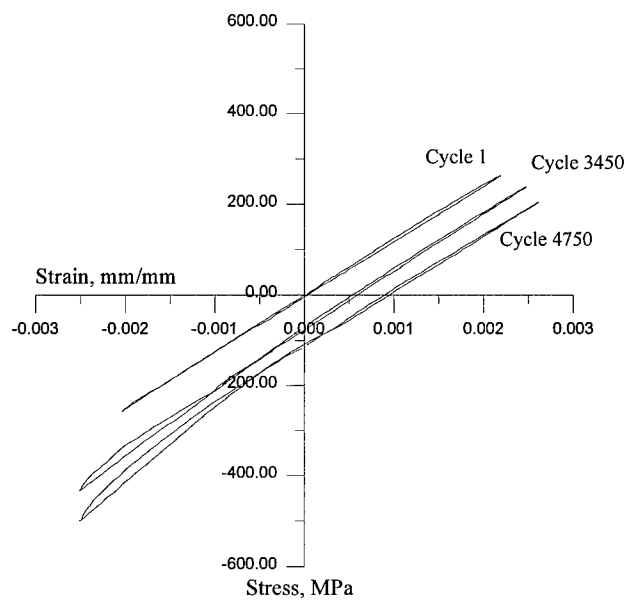
Figure 32. Stress vs. Strain Curves, 0.25% Maximum Strain, 50% Expected Life

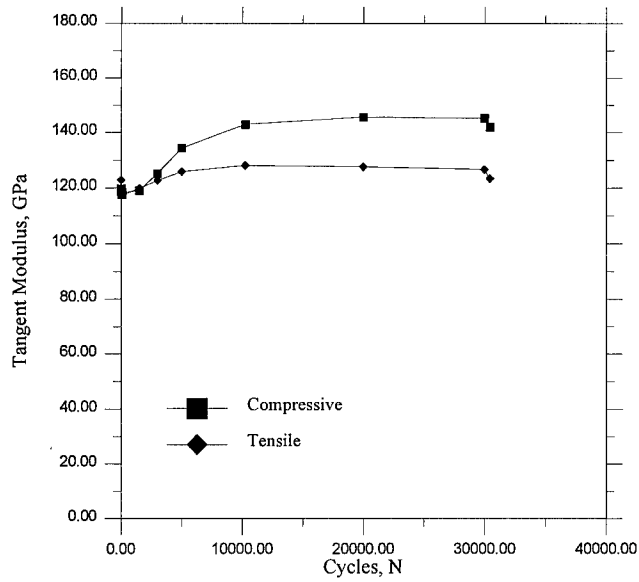from 0.25% to 0.4%. In such a narrow range, it is not unusual to find similarities in the fracture mechanisms of these specimens. Most of them displayed multi-tiered topography which developed from matrix cracks which coalesced at different planes along the weak fiber-matrix interfaces. This behavior is common of specimens tested at low strain levels like the ones in this test, and was observed by Sanders and Mall [24] . Damage mechanisms also exhibited a number of cracks which initiated at the 90°fibers, propagated transversely to the 0°fibers and caused debonding of the 0°ply fiber/matrix interface.

During this analysis, the following two damage mechanisms are of great importance: brittle cleavage and ductile fracture. Cleavage fracture occurs by direct separation along crystallographic planes due to a simple breaking of atomic bonds. The flat cleavage facets through the grains have a high reflectivity, giving the cleavage fracture a bright shiny appearance. Ductile fracture occurs when the material's intermediate-size particles lose their cohesive bond with the surrounding matrix due to their inability to deform during plastic flow. When this takes place, microvoids are formed. The voids grow by slip, the material between voids neck down and adjacent voids coalesce spreading the fracture. These coalesced voids result in the dimpled surface which is distinctive of ductile fracture.

Before drawing any conclusions about the damage mechanisms experienced by the specimens at the different strain levels, it is important to remember the steps involved on a residual strength test. First, the specimens are fatigued to a certain percentage of their expected lives, then they are monotonically pulled to failure. During the initial part of

50

this process, the specimens experience the fatigue damage mechanisms peculiar to the maximum strain level and the number of cycles they are exposed to. This damage mechanism is therefore expected to be different between a specimen exposed to 0.25% maximum strain, for 25% of its expected life, and one exposed to 0.4% maximum strain, for 75% of its expected live. However, when these two specimens are monotonically pulled to failure, they both experience a similar phenomenon. The matrix cracks, developed during cycling, grow rapidly around or through the fibers, transferring the monotonic tensile load to the remaining fibers and matrix which had not been previously broken. The portion of the matrix which is broken by the monotonic load will most likely reflect ductile void fracture when observed under the SEM; that broken during the cyclic portion of the test, most likely will reflect a brittle cleavage failure. Therefore, the presence of ductile voids on a fracture surface will hereafter be associated with failure due to monotonic load. The presence of brittle cleavage, in turn, will be associated with fatigue matrix cracks which developed during cycling. The main concern of this section is to understand the amount and type of damage the specimens experienced prior to beginning the monotonic residual test.

In a previous research conducted by Talreja [25] , the S-N curve was divided into three different regimes based on the dominant failure mechanism. He tested an unidirectional, SCS-6/Ti-15-3 laminate, in tension-tension fatigue at a R-ratio of 0.1 and concluded that, in Regime 1 failure occurred due to fiber overload, in Regime 2 due to matrix cracking and in Regime 3 matrix cracks did not initiate. Based solely on Talreja's study, and the stress range of the current work, our specimens, prior to the monotonic

load portion of the test, belong to Region 2 where matrix crack is the dominating damage mechanism. However, due to the variances in the fatigue behavior of the cross-ply some of them could fall somewhere in between Regions 1 and 2 where a mixed-mode is present. This mixed-mode transition region was studied by Boyum [1] in a previous study where she defined it as Region 2a.

4.2.1 0.4% Maximum Strain

Figure 33 shows an overall view of the fracture surface of the 75% coupon which, upon examination, confirmed the fracture of several 0° fibers and a combination of ductile void coalescence and brittle cleavage; the former being present over approximately 10% of the fracture surface. The dimpled surface seen on a portion of the specimen is indicative of a fiber-dominated tensile overload type of failure. In other words, at the time the monotonic load was applied, about 10% of the fracture surface had not experienced matrix cracking and failed under the monotonic load. Figure 34 illustrates this combination of brittle and ductile fracture mechanisms. Most of the matrix-fiber debonding on this specimen took place in areas perpendicular to the applied strain in the 90° ply.

Also Figure 34 depicts a portion with rough appearance on the fiber surface; this porousness can be attributed to oxidation. As the cracks developed during fatigue loading, oxygen was able to reach the fibers producing oxidation at elevated temperature. No longitudinal cracks were observed on this specimen, however, examination of the polished surface shown in Figure 35 showed a small number of fibers fractured perpendicularly to the load direction. It is difficult to say, with any degree of certainty, whether these fibers broke during cycling or when the monotonic load was applied.
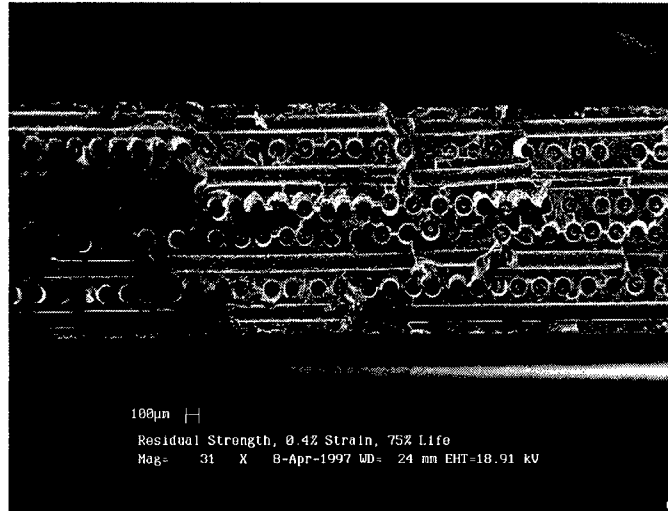
Figure 33. Fracture Surface, 0.4% Maximum Strain, 75% Expected Life
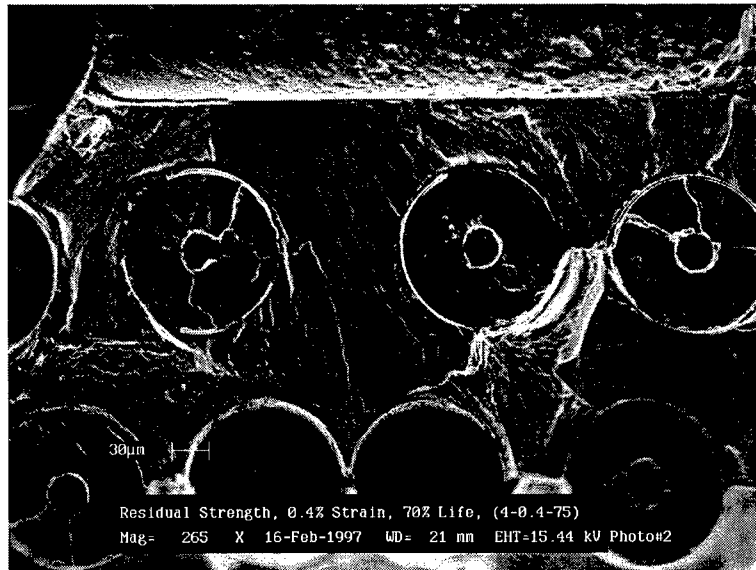
Figure 34. Ductile and Brittle Fracture, 0.4% Maximun Strain, 75% Expected Life
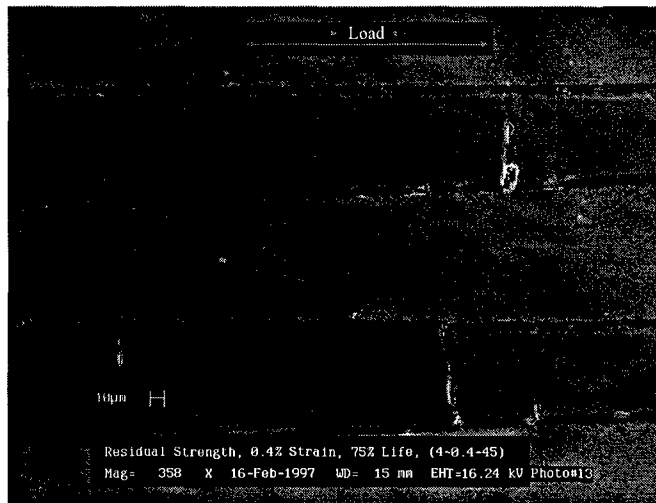
Figure 35. Cross Sectional Area Depicting Fiber Fracture, 0.4% Maximum Strain, 75% Expected Life

The fracture analysis of the 50% expected life coupon indicated a similar damage mechanism as that of its predecessor, however, the percentage of ductile void on the surface was approximately 20%. The permanent oval shape of the matrix surrounding the fibers in Figure 36, indicated the presence of ductile necking plasticity. The dimples on the matrix corroborate this assumption since they are formed during void coalescence and are characteristic of a ductile fracture. The gap between the fibers and matrix seen in the polished cross-section, shown in Figure 37, depicts some of the fiber-matrix debonding in the 0° plies which was present in this specimen.
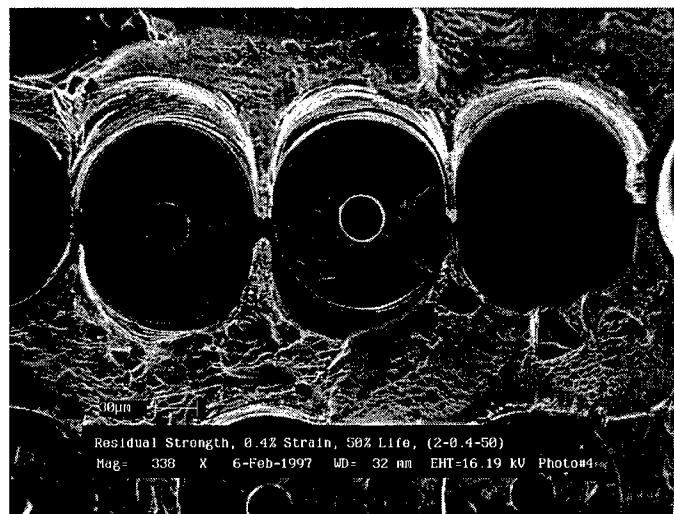
Figure 36. Matrix Plasticity and Ductile Fracture, 0.4% Maximum Strain, 50% Expected Life

Figure 38 shows an overall view of the 25% life expectancy coupon which displays similar multi-tiered topography as previous tests, but 90% of the surface consists of ductile void type of fracture. The fracture surface in Figure 39, revealed several 0° fibers broken through the middle indicating that the compressive load could have caused radial fiber cracking. There was also enough compressive stress to cause debonding
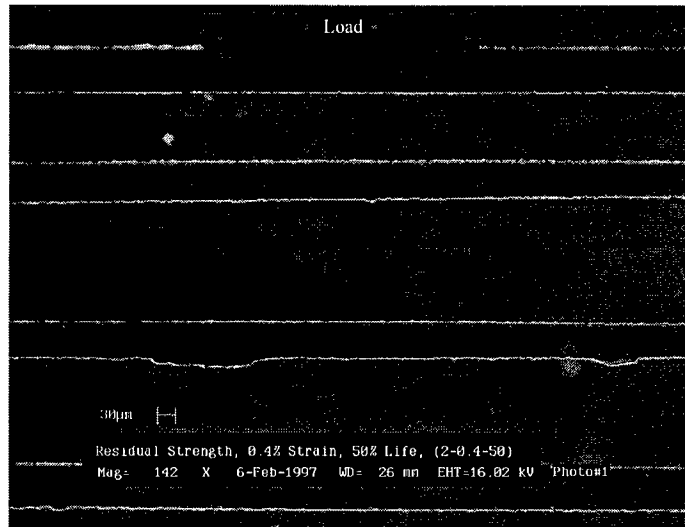
Figure 37. Fiber-Matrix Debonding, Cross Sectional Area, 0.4% Maximum Strain, 50% Expected Life
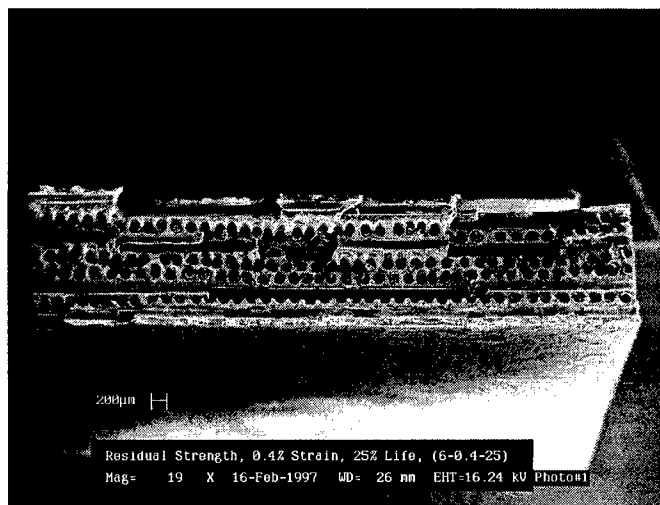
Figure 38. Overall View of Fracture Surface, 0.4% Maximum Strain, 25% Expected Life

along the interface of the metal foils used during fabrication. Evidence of fiber failure, common to most of the 0.4% maximum strain tests, is shown in Figure 40.
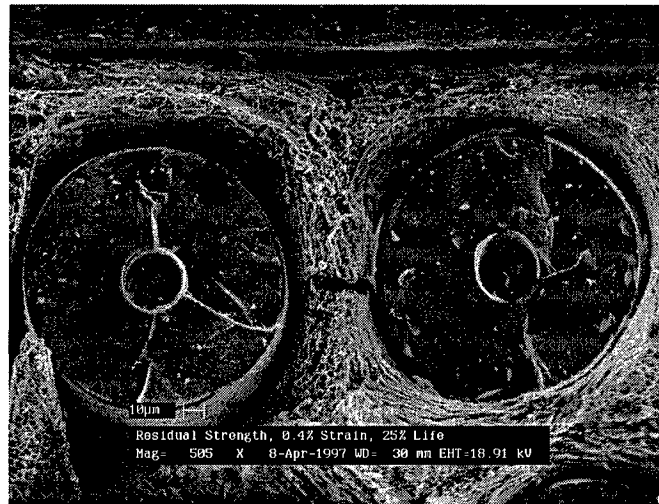
Figure 39. Fiber Radial Crack, 0.4% Maximum Strain, 25% Expected Life

4.2.2 0.3% Maximum Strain

The 0.3% maximum strain tests, which will be discussed in this section, also reflect a combination of fiber and matrix damage mechanisms. In comparison to the 0.4% maximum strain tests, this group exhibited a slight decrease of matrix plasticity and ductile void coalescence. This set of tests, as it will be shown later, will provide a logical middle step in the behavioral pattern between the 0.4% and 0.25% maximum strain tests. The fracture surface for the 75% expected life is shown in Figure 41 and, as it can be seen, the surface consists of approximately 20% ductile failure mechanism. Figure 42 is a good representation of the ductile failure portion of the coupon. At this strain level matrix cracks played a more significant role in the damage of the matrix than on the previous test. The channels seen in the upper layer of the fracture surface are created as

57

Figure 40. Fiber Failure, 0.4% Maximum Strain, 25% Expected Life

the fiber-matrix interface failed and the 90° fibers were pulled away. This pull-out was frequently seen during this study and is characteristic of a cross-ply failure. Although 20% of the fracture surface on this coupon involved ductile fracture, Figure 43 shows a region which represents the remaining 80% of the surface where brittle cleavage fracture of the matrix was present.
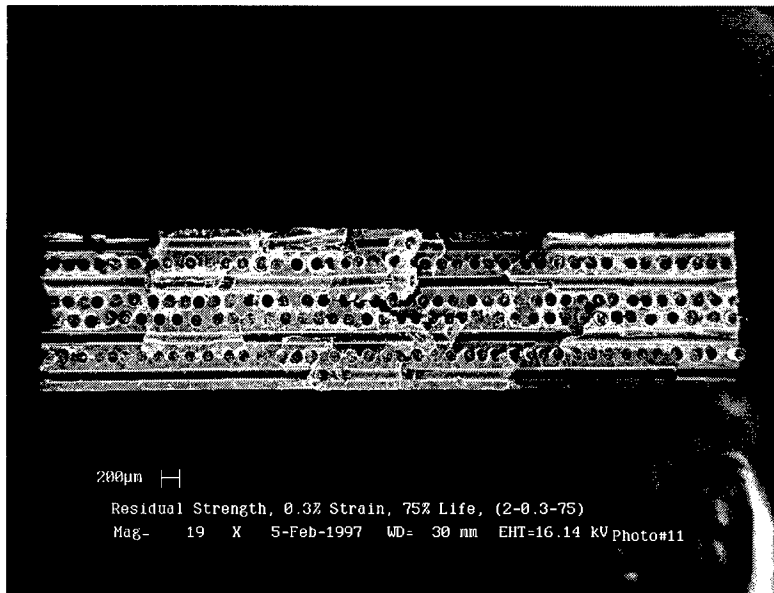
Figure 41. Fracture Surface, 0.3% Maximum Strain, 75% Expected Life

The fracture surface depicted in Figure 44 belongs to the 12% expected life specimen and reflects numerous cracks, the majority of which initiated from the 90° fibers and then propagated through the matrix. The stepped fracture surface indicates that damage was accumulating in several planes within the specimen. The percentage of ductile void on this surface is about 80%. As will be seen in the next section, this fracture topography was also seen in the 0.25% maximum strain specimens.
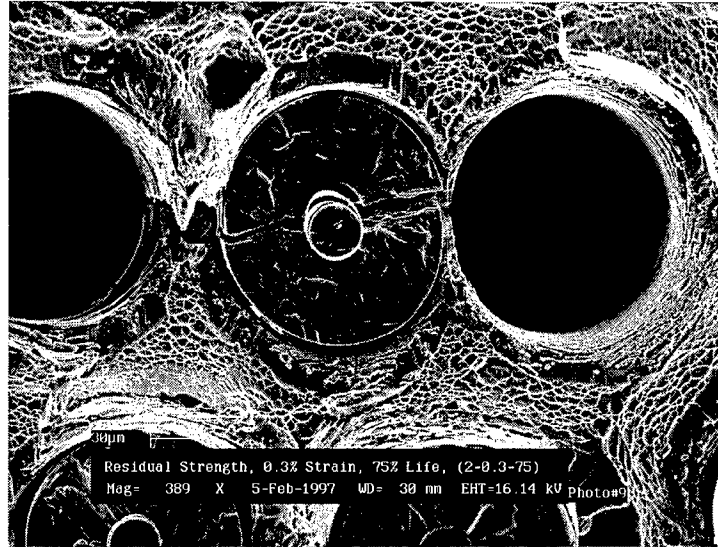
Figure 42. Ductile Void Coalescence Fracture Surface, 0.3% Maximum Strain, 75% Expected Life
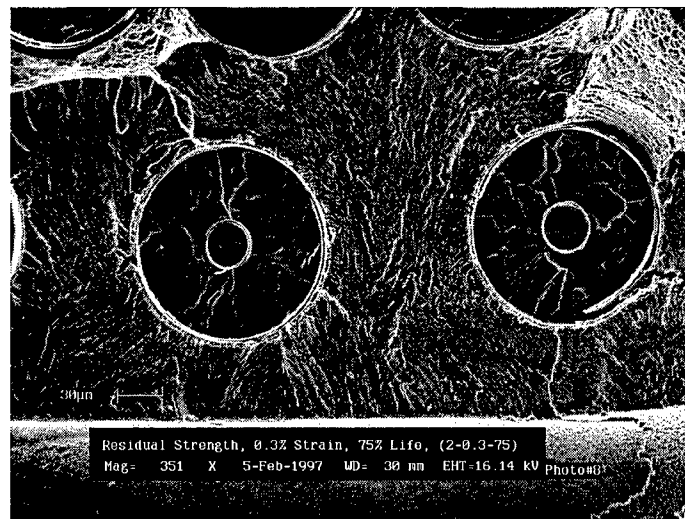
Figure 43. Brittle Fracture Surface, 0.3% Maximum Strain, 75% Expected Life
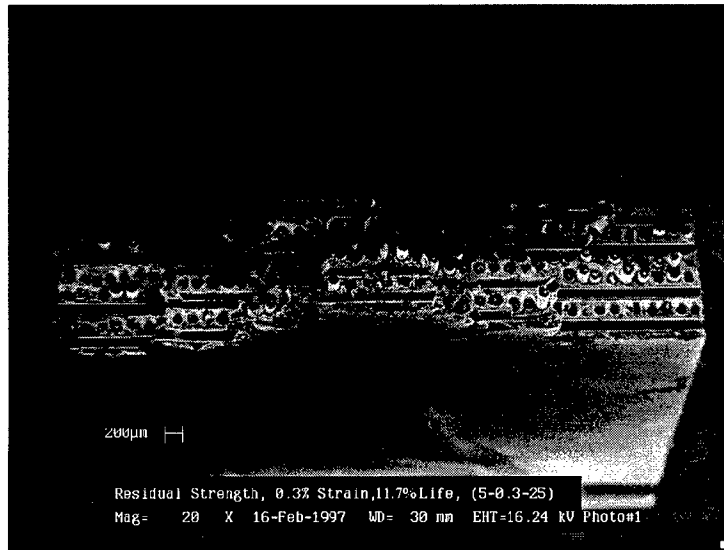
Figure 44. Fracture Surface, 0.3% Maximum Strain, 12% Expected Life

4.2.3 0.25% Maximum Strain

The specimen, seen in Figure 45, does not reflect a dominant crack plane. It shows several major cracks which originated at the 90° fiber interface and finally coalesced to failure upon tension overload. The surface reflects approximately 20% ductile void, which means that 80% of the matrix surface experienced cracking during cyclic loading. This observation is not unusual for this strain level due to the large number of cycles the specimen is exposed to. During a long cyclic loading test, as that of the current strain level, cracks have sufficient time to grow and propagate through the matrix. Most of the cracks initiated at the 90° fibers and propagated transversely to the 0° fibers, causing debonding of the fiber/matrix interface. Furthermore, similar to specimens from the 0.4% maximum strain level, this coupon also showed signs of oxidation, as seen in Figure 46.
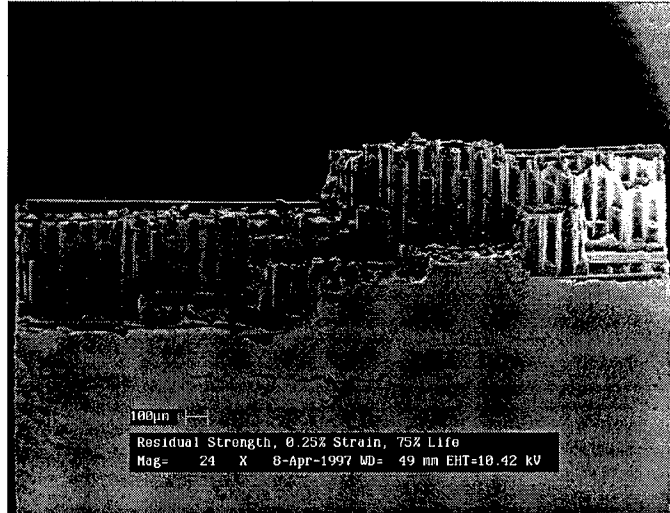
Figure 45. Overall View of Fracture Surface, 0.25% Maximum Strain, 75% Expected Life
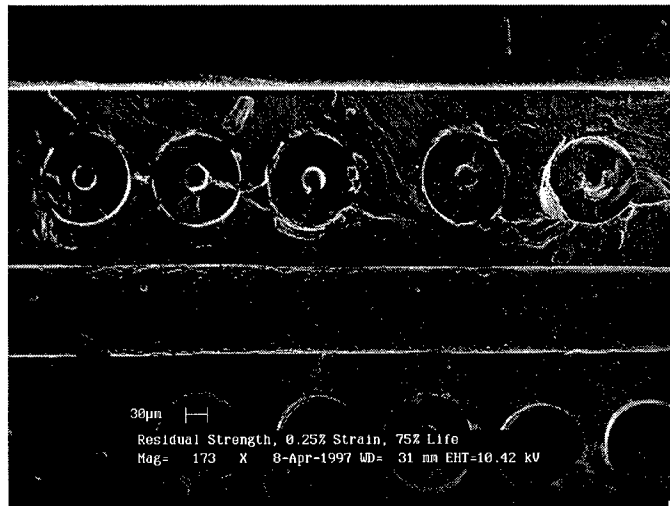
Figure 46. Oxidation of Fracture Surface, 0.25% Maximum Strain, 75% Expected Life

5. Residual Strength Analysis and Discussion

5.1 Current Work

As previously mentioned, the objective of this research was to investigate the residual strength of a cross-ply, $[0/90]_{2s}$, SCS-6/Ti-15-3 MMC at elevated temperature (427°C) when exposed to fatigue loading. This chapter will discuss the residual strength behavior of tests conducted in this study at different strain levels, and then compare them to previous works which have been performed on unidirectional specimens and also under load controlled mode.

Prior to proceeding with comparisons between current work and previous data, it is important to lay the foundation for this chapter by briefly discussing the differences, or similarities, among the three groups of tests conducted in this work. These are shown in Figure 47, where normalized residual strength is plotted as a function of normalized cycles. Here the normalization is done with the ultimate strength from Chiou's work [4] and the fatigue life from Dennis'work [7] . In Figure 47, it is observed that the normalized residual strength of the different strain groups fell on a narrow scatter band, gradually decreasing with increasing number of cycles at a very similar rate. There is a linear relationship between the normalized residual strength and normalized cycles at all strain values. This linear relationship is a very interesting phenomenon which does not seem to be previously observed. As will be shown later, this relationship does not seem to hold on a load controlled mode.

Figure 48 shows the normalized residual strength in terms of the actual number of cycles. This plot suggest a direct relationship between the residual strength degradation
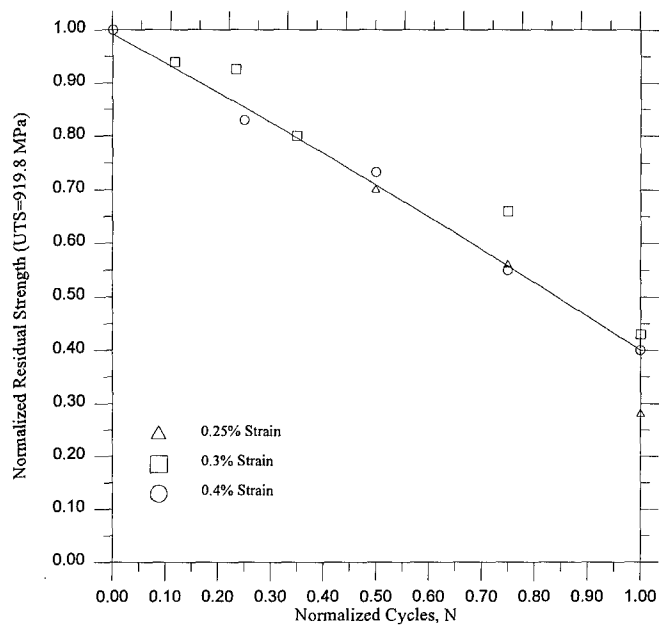
Figure 47. Normalized Residual Strength vs. Normalized Number of Cycles-Current Work

and the number of cycles with the former degrading inversely proportional to the latter. In order to establish a correlation between the residual strength degradation and the number of cycles, the damage accumulation in terms of the percentage of ductile void present on the different fracture surfaces has been plotted as a function of the number of cycles in Figure 49. It can be seen here that the percentage of ductile void, similar to the residual strength, decreases with the number of cycles. As discussed in Chapter 4, the presence of brittle cleavage is associated with matrix cracks (damage accumulation) prior to the monotonic load, and the presence of ductile void with failure due to the monotonic load. Therefore, it is concluded that the residual strength degradation depends on the amount of matrix damage, and the matrix damage, in turn, depends on the number of cycles. From Figure 49 it can also be observed that the slope of the ductile void percentage vs. number of cycles curve decreases with decreasing maximum strain. This suggests that as the maximum strain decreases, the damage mechanism is more matrix dominated thus reflecting a smaller percentage of ductile void. This is expected since at lower strain levels the specimen is subjected to more cycles for a given percentage of fatigue life.

To further understand the relationship between damage accumulation and residual strength degradation, the Young's modulus behavior for three representative samples was plotted against number of cycles. The drop in Young's modulus, seen during the early portion of the individual curves in Figure 50, corresponds to the initial damage experienced by the specimens. Following this initial drop, the Young's modulus behavior does not differ greatly among the three specimens until near the end of the tests. This
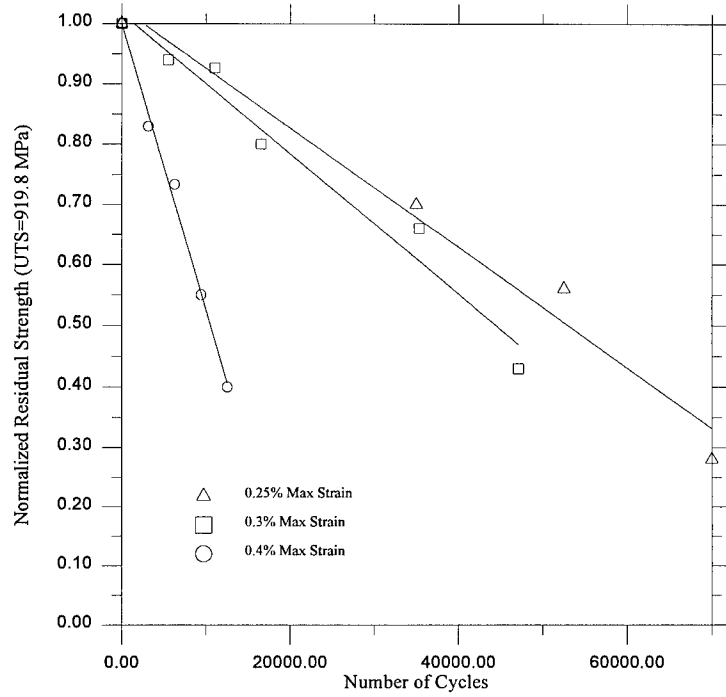
Figure 48. Normalized Residual Strength vs. Number of Cycles-Current Work
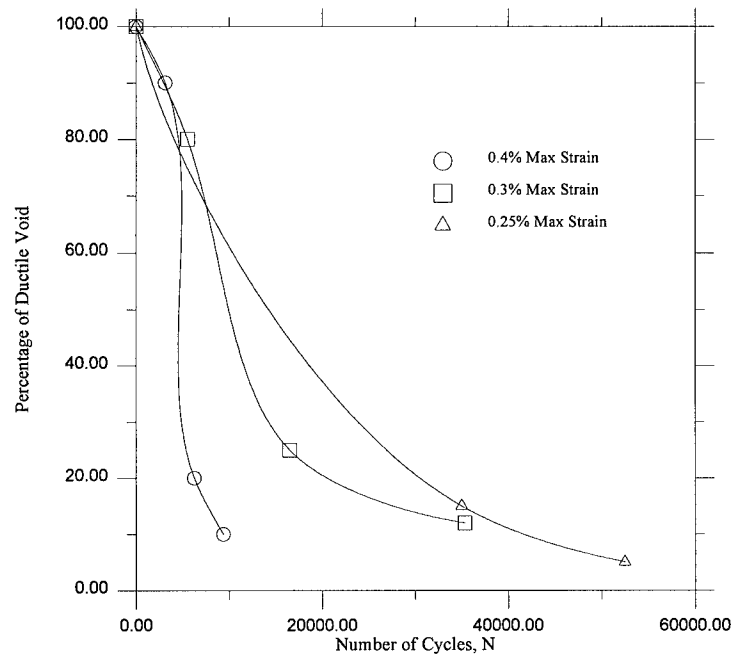
Figure 49. Percentage of Ductile Void on Fracture Surface vs. Number of Cycles

67

similarity in the Young's modulus behavior can be attributed to the small strain range under which these specimens were tested. Although the amount of damage accumulation is slightly different among the separate strain levels, this difference is not large enough as to significantly affect the Young's modulus behavior.
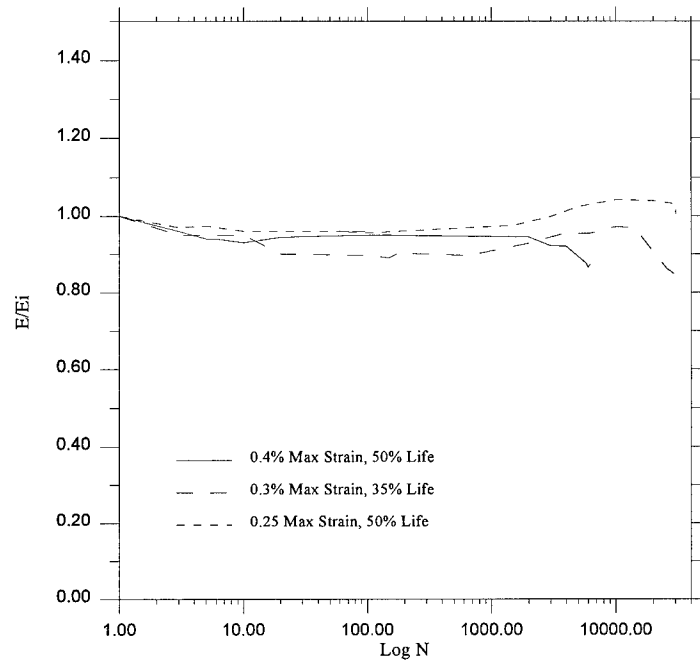
Figure 50. Young's Modulus vs. Number of Cycles

5.2 Load vs. Strain Controlled Modes

In this section a comparison will be made between the residual strength behavior of the cross-ply, SCS-6/Ti-15-3, MMC, under strain controlled mode, from the current work and that conducted by Chiou under load controlled mode [4] . To accomplish this, the data obtained in the current study were plotted in Figure 51 together with previous data from Chiou. The residual strength obtained in this study was normalized

using Chiou's ultimate tensile strength value of 919.82 MPa which is the average of the monotonic test results that he conducted on his cross-ply MMC [4] .

The 0.4% maximum strain test results from the current study fall almost on top of the 450 MPa results of Chiou's [4] . The present tests were conducted at a frequency of 0.0625 Hz., Chiou's 450 MPa test, in turn, was conducted at 10 Hz. The 75%, 50% and 25% expected life from the current work consisted of four data with 17,023, 10,692, 8,004 and 6,598 cycles and corresponded to Chiou's 9,375, 6,250 and 3125 cycles respectively. In comparing the above mentioned tests, it can be observed that the data from these two groups tends to collapse when plotted on a normalized cycles. This behavior may be due to the fact that Chiou's 450 MPa test corresponded to a maximum strain of 0.37% based on an average initial modulus of 122 GPa. The strain control mode residual strengths do show a slightly greater and more consistent degradation than its counterpart from the load controlled mode as seen in Figure 51. This may be attributed to the frequency and R-ratio differences between these two studies [3] . As the frequency increases, so does the matrix damage, however, creep and the amount of fiber cracks decreases [21] . What this shows is that the tests corresponding to a frequency of 0.0625 Hz experienced the equivalent amount of damage to those at 10 Hz at a much smaller number of cycles. This relationship of damage mechanism and frequency on MMC was also studied by Nicholas et. al.[19] . Furthermore, looking at the fracture surfaces of Chiou's 450 MPa and current work's 0.4% maximum strain, one can observe a flatter surface on the former compared to the multi-tiered surface of the latter, indicating a

69

greater matrix crack influence on the failure mechanism of the current work's specimen vs. that from Chiou.

Similar observation can be made for the 0.3% maximum strain tests from the current work when compared with Chiou's 300 MPa test. The frequency for the 0.3% maximum strain tests was 0.0833 Hz and its 35%, 23% and 12% expected lives tests corresponded to 16,500, 11,000 and 5,500 cycles in Chiou's tests, respectively. Chiou's 300 MPa test corresponded to a maximum strain of 0.25%. Along with the frequency and R-ratio observations made earlier, the current work tests had less cycles than those of Chiou's 300 MPa. This explains in part the limited amount of damage and the high residual strength. Combined results of Chiou's and current work is shown in Table 3.
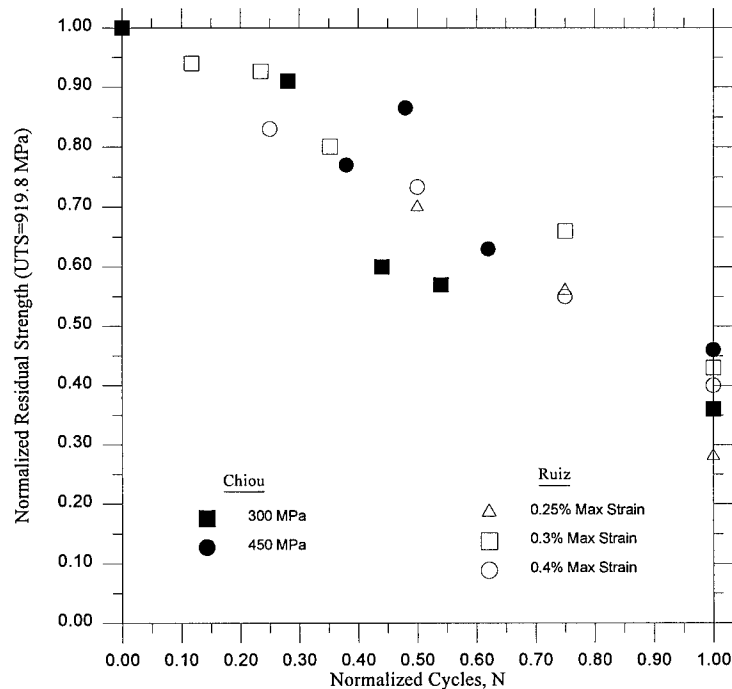

Figure 51. Normalized Residual Strength vs. Normalized Cycles of a Cross-Ply Laminate Under Strain and Load Controlled Modes

Another observation worth making about Figure 51 is the fact that the data have the tendency to converge as the fatigue cycles increase. This trend was also observed under load controlled tests run by Dennis [7] and can be attributed to the fact that, in this region of matrix dominated failure, both load and strain controlled modes provide similar fatigue lives.

Upon observing the different fracture surfaces from this study, it was seen that most of the cracks leading to specimen failure originated at the 90° fibers and then extended towards the 0°. Matrix-fiber debonding was the primary fatigue fracture mechanism. Chiou made similar conclusions in his work while testing the same type of cross ply MMC under load controlled, tension-tension mode [4]. This similarity in the fracture mechanism of load vs.strain controlled tests was expected. Previous works conducted by Jackson [10], Boyum [1] and Dennis [7] have shown that the fatigue damage mechanisms of cross-ply MMC tested under strain control will be the same as those tested under load control at the same stress ratio.

5.3 Unidirectional vs. Cross-Ply

To better understand the behavior differences between the unidirectional and the cross-ply laminates, it is important to remember the effects of the fiber-matrix interface debonding on the modulus degradation as discussed in Chapter 4. In that chapter the main differences in the failure mechanisms of the low strain test, 0.25% maximum strain, and its counterpart the 0.4% maximum strain were established. It was concluded that the former test was very dependent on the accumulation of matrix damage while

Table 3. Residual Strength Data from Current and Previous Studies, Strain and Load Controlled Mode

Control Mode	Max Strain	Max Stress (MPa)	Number of Cycles	Frequency (Hz)	Residual Strength (MPa)
Strain	0.25%	n/a	35,000	0.1	647
Strain	0.25%	n/a	17870	0.1	572
Strain	0.3%	n/a	16,500	0.083	736
Strain	0.3%	n/a	11,000	0.083	852
Strain	0.3%	n/a	5,500	0.083	865
Strain	0.4%	n/a	9,375	0.062	510
Strain	0.4%	n/a	6,250	0.062	670
Strain	0.4%	n/a	3,125	0.062	761
Load*	n/a	450	6,598	10	768
Load*	n/a	450	8,004	10	859
Load*	n/a	450	10,692	10	663
Load*	n/a	450	17,023	10	450
Load*	n/a	300	50,010	5	767
Load*	n/a	300	80,010	5	512
Load*	n/a	300	100,010	5	481
Load*	n/a	300	186,000	5	300
Note: * From Chiou [4]					

the latter depended heavily on the fibers. It was also established a direct association between the amount of matrix damage, residual strength and number of cycles.

Keeping the above premise in mind, it can easily be assumed that the matrix in the unidirectional laminate will not experience as much initial damage as in the cross-ply laminate since it lacks the crack initiation sites of the 90° plies. Since damage accumulation is much slower in the unidirectional laminate, so is its residual strength degradation. Figure 52 shows the residual strength of the current work and those of unidirectional coupons, performed by Calcaterra [3] , which were tested under the same control mode, temperature and R-ratio. As can be seen from this graph, the unidirectional specimens maintained a higher residual strength for a longer portion of their cyclic lives (up to 80% of fatigue life). The cross-ply, in turn, shows a consistent reduction in residual strength even after little exposure to fatigue (i.e. even at 25% of fatigue life) which continued in linear fashion until the end.

The residual strength dependency on damage mechanism and the damage mechanism dependency on number of cycles discussed earlier, are also important factors in the comparison of cross-ply and unidirectional materials. Figure 53 shows the normalized residual strength of both unidirectional and cross-ply laminates as a function of cycles under both loading modes. From this graph it can be seen that the 0.3% maximum strain tests, in both cases, reflect very different residual strengths for similar number of cycles. The reason for this behavior lies in the matrix damage dependency of the residual strength at this strain level. In turn, the 0.4% maximum strain, which depends more on

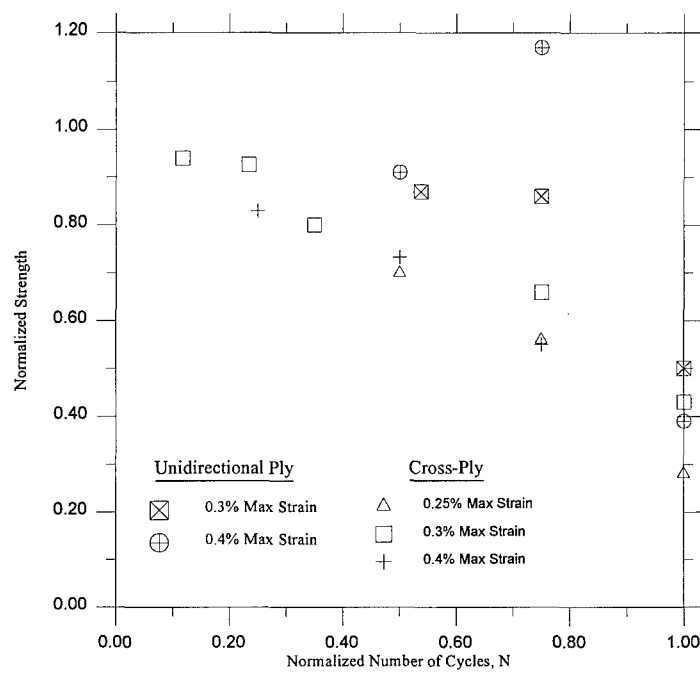Figure 52. Normalized Residual Strength vs.Normalized Number of Cycles for Unidirectional and Cross-Ply Laminates Under Strain Controlled Mode

the fibers, reflect more similar residual strength behavior for both types of tests. The

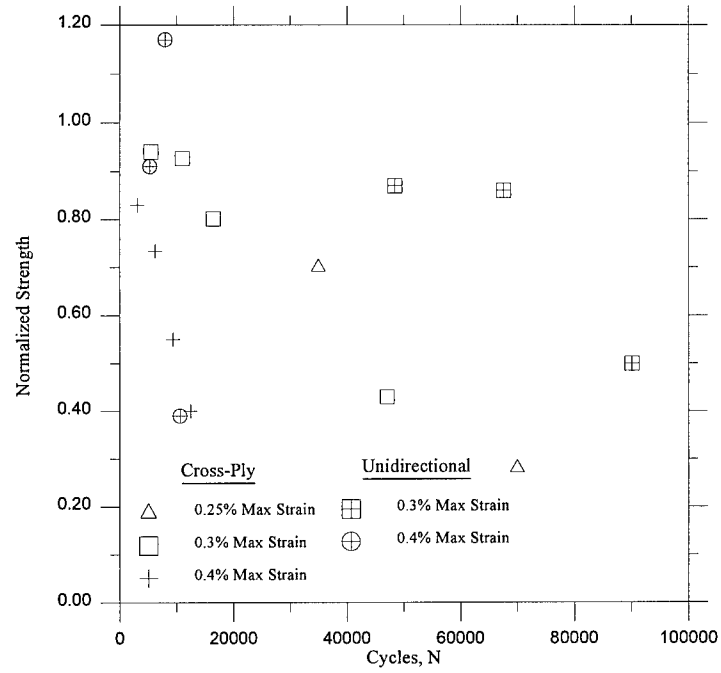data used in Figures 52 and 53 is given in Table 4.

Figure 53. Normalized Strength vs.Cycles for Unidirectional and Cross-Ply Laminates Under Strain Controlled Mode

Table 4. Residual Strength Data from Current and Previous Studies for Cross-Ply and Uni-directional Laminates Under Strain Controlled Mode

Max Strain	Number of Cycles	Frequency (Hz)	Residual Strength (MPa)
0.25%	35,000	0.1	647
0.25%	17,870	0.1	572
0.3%	16,500	0.083	736
0.3%	11,000	0.083	852
0.3%	5,500	0.083	865
0.4%	9,375	0.062	510
0.4%	6,250	0.062	670
0.4%	3,125	0.062	761
0.3% *	48,464	0.083	1,249
0.3% *	67,552	0.083	1,232
0.3% *	90,069	0.083	728
0.4% *	5,315	0.062	1,310
0.4% *	7,973	0.062	1,673
0.4% *	10,630	0.062	563
Note: * From Calcaterra [3]			

6. Conclusions and Recommendations

The objective of this study was to investigate the residual strength of a cross-ply, [0/90]$_{2s}$, SCS-6/Ti-15-3, metal matrix composite at elevated temperature when exposed to fatigue loading under strain controlled mode. Although many studies have been conducted in the characterization process of this material, this is the first known research performed on the residual strength of this MMC under strain controlled, fully-reversed tension-compression fatigue.

The three groups of tests were conducted at different strain levels in order to establish the differences, or similarities, among the residual strengths at different strain levels. It was observed that the normalized residual strength of the different strain groups fell on a narrow scatter band, gradually decreasing with increasing number of normalized cycles at a very similar rate. The percentage of ductile void on the fracture surface also decreased with increasing number of cycles which suggested that damage accumulation increased with the number of cycles, and that the residual strength degraded with damage accumulation.

The current results were compared with that of a previous study conducted by Chiou under load controlled mode [4] . This comparison showed a slightly different pattern such that the residual strength under strain controlled degraded earlier and more than its counterpart under load controlled mode. Previous works conducted by Jackson [10] , Boyum [1] and Dennis [7] have shown that the fatigue damage mechanisms of cross-ply MMC tested under strain control will be the same as those tested under load control at the same stress ratio. The differences between Chiou's and current work was,

77

therefore more likely, due to the frequency and R-ratio differences between these two studies.

The residual strength degradation of the cross-ply and that of an unidirectional laminates were also compared. A significant difference in the residual strength degradation behavior between them was found which was brought about by the differences in ply orientation. Due to the lack of 90° plies, and its crack initiation propensity, the matrix in the unidirectional laminate did not experience as much initial damage as in the cross-ply laminate. The unidirectional specimens, therefore, maintained a higher residual strength for a longer portion of their lives. The cross-ply, in turn, showed a gradual decline in residual strength from the beginning of the test.

The microscopic evaluation of the specimens revealed signs of oxidation at every strain level tested. This oxidation may have had a detrimental effect on the residual strength degradation of the material. Further studies should be conducted in a vacuum chamber to quantify the effects of oxidation on this material.

Although this work contributed to a better understanding of the residual strength degradation of MMCs, more testing is needed to fully characterize the residual strength behavior of this material. For instance, while comparing the load controlled vs. strain controlled tests earlier in this work, it was determined that the difference in frequency and R-ratio may have an effect on the residual strength differences between both of these tests. Thus, it is recommended that further testing be conducted at both strain and load controlled modes using the same R-ratio, frequency, etc. Furthermore, in the area of material preparation for future tests, the author recommends that dogbone specimens

be used in place of the rectangular coupons to minimize the chances of failure outside

the extensometer area.

APPENDIX A Additional Data

This Appendix contains additional data not presented previously in this document. It includes plots of the maximum and minimum strain behaviors, the secant modulus and monotonic tests stress/strain plots of the different strain levels.
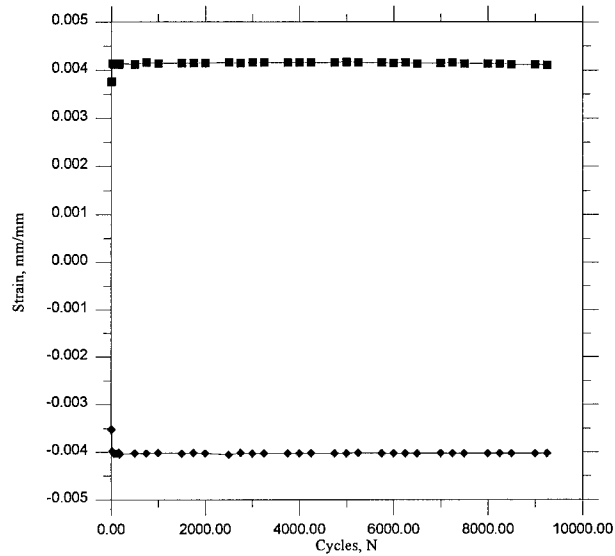

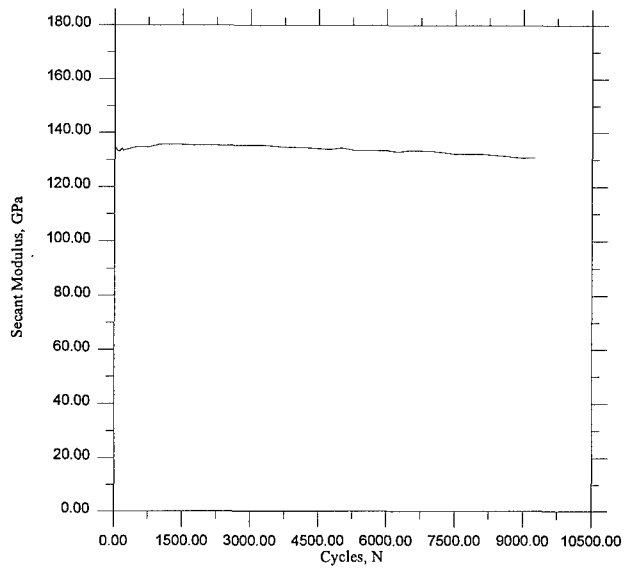Figure 54. Maximum and Minimum Strain, 0.4% Maximum Strain, 75% Expected Life

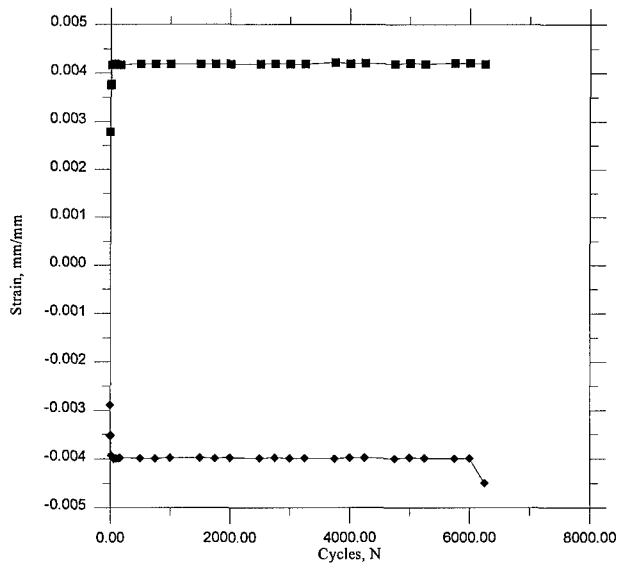Figure 55. Secant Modulus, GPa, 0.4% Maximum Strain, 75% Expected Life

Figure 56. Maximum and Minimum Strain, 0.4% Maximum Strain, 50% Expected Life
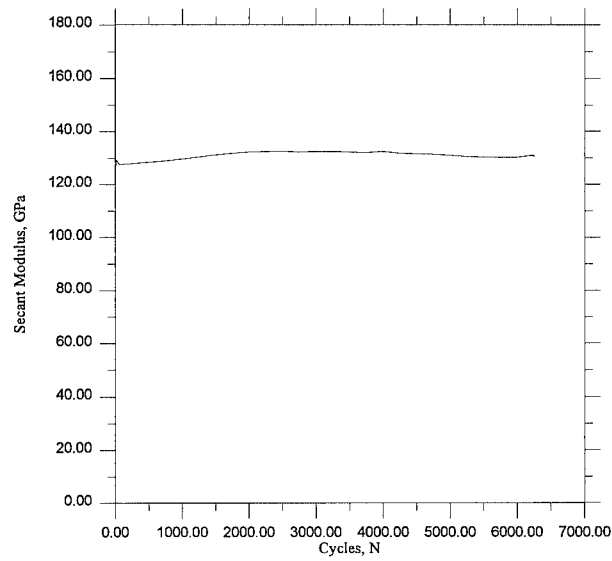
81

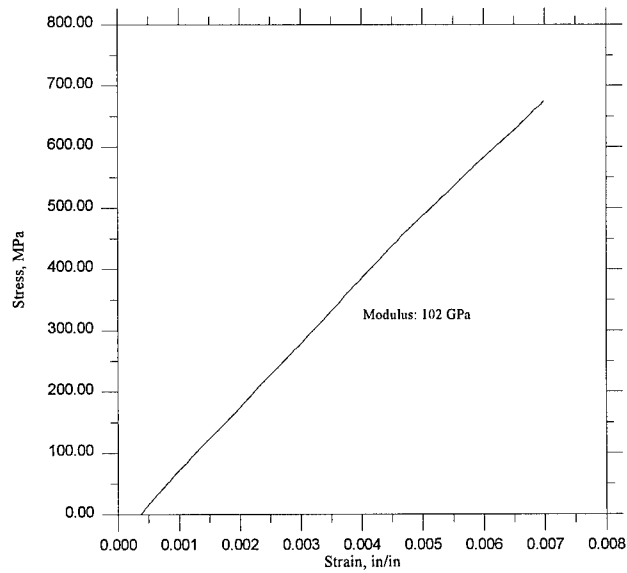Figure 57. Secant Modulus, 0.4% Maximum Strain, 50% Expected Life

Figure 58. Monotonic Test to Failure, 0.4% Maximum Strain, 50% Expected Life

Figure 59. Maximum and Minimum Strain, 0.3% Maximum Strain, 35% Expected Life

Figure 60. Secant Modulus, GPa, 0.3% Maximum Strain, 35% Expected Life

83

Figure 61. Monotonic Test to Failure, 0.3% Maximum Strain, 35% Expected Life

Figure 62. Maximum and Minimum Strain, 0.3% Maximum Strain, 23% Expected Life

84

Figure 63. Secant Modulus, GPa, 0.3% Maximum Strain, 23% Expected Life

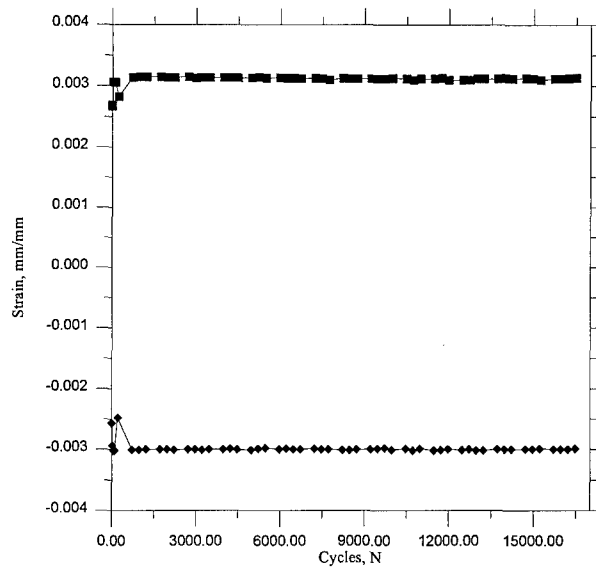Figure 64. Monotonic Test to Failure, 0.3% Maximum Strain, 23% Expected Life

Figure 65. Maximum and Minimum Strain, 0.3% Maximum Strain, 12% Expected Life

Figure 66. Secant Modulus, GPa, 0.3% Maximum Strain, 12% Expected Life

86

Figure 67. Monotonic Test to Failure, 0.3% Maximum Strain, 12% Expected Life

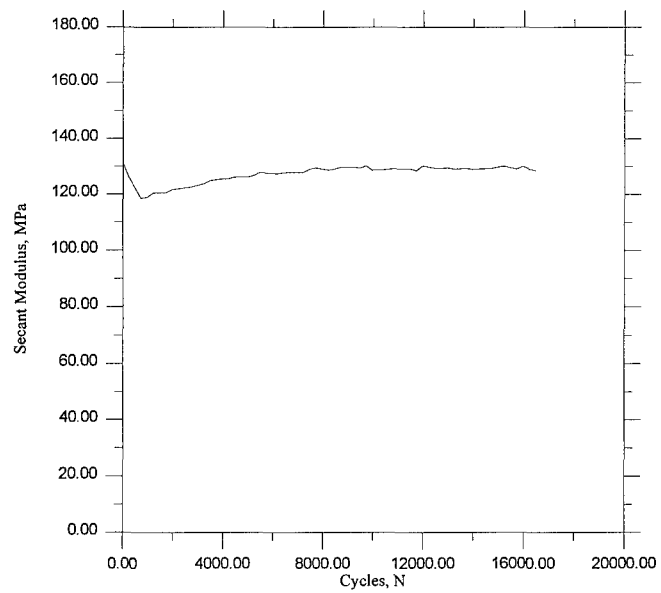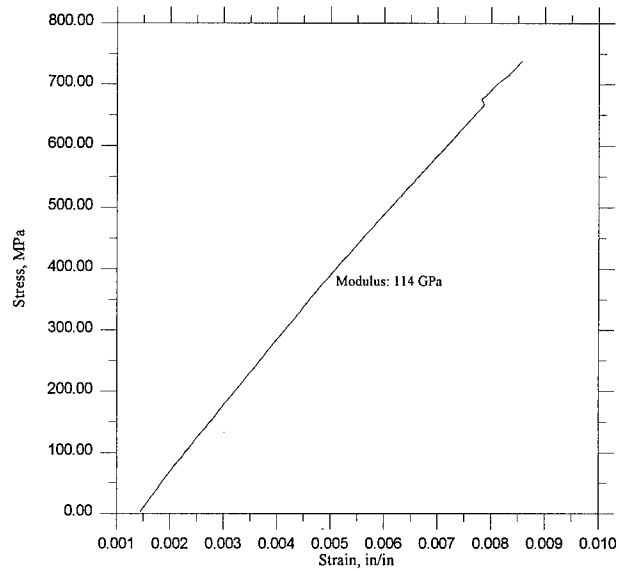Figure 68. Maximum and Minimum Strain, 0.4% Maximum Strain, 25% Expected Life

87

Figure 69. Secant Modulus, GPa, 0.4% Maximum Strain, 25% Expected Life

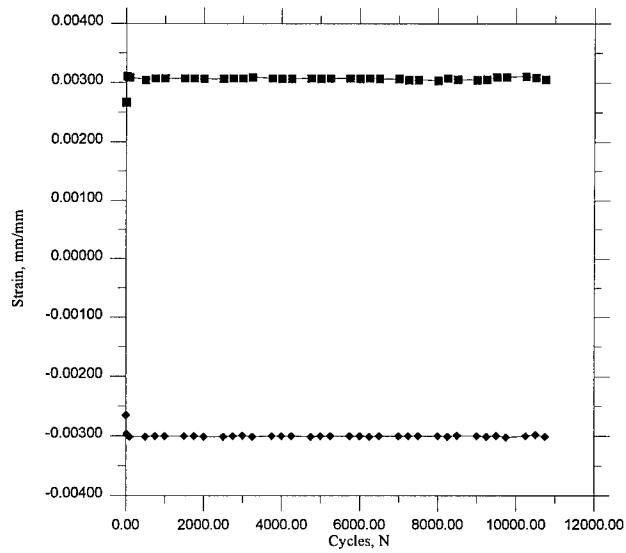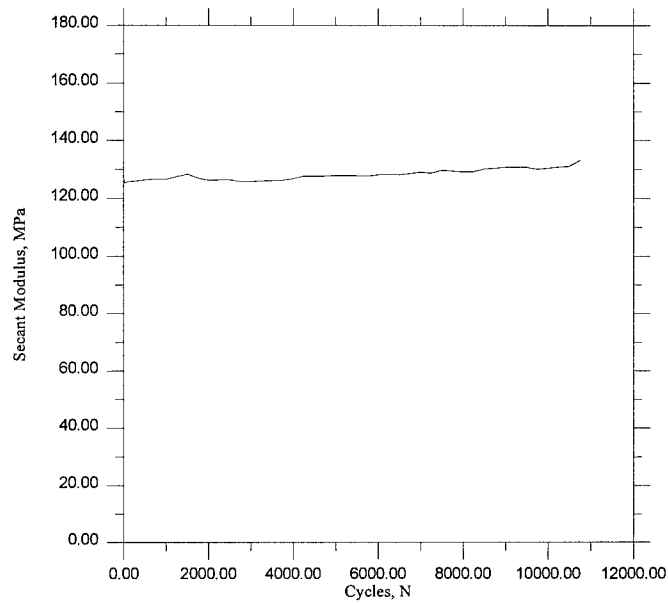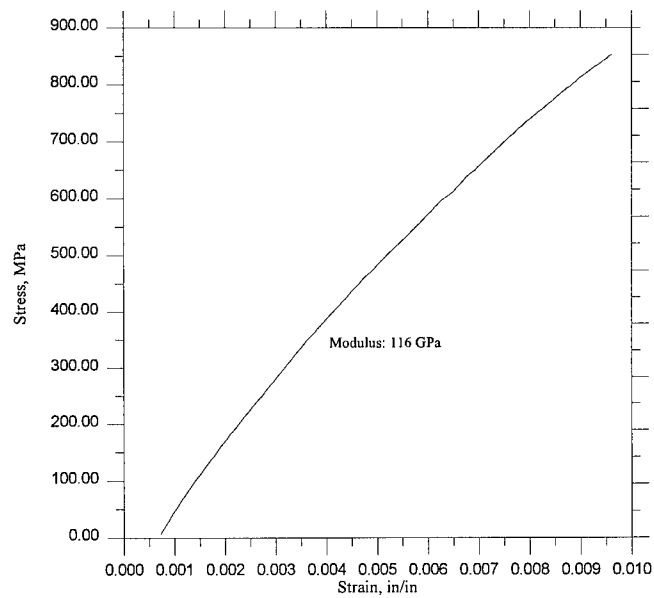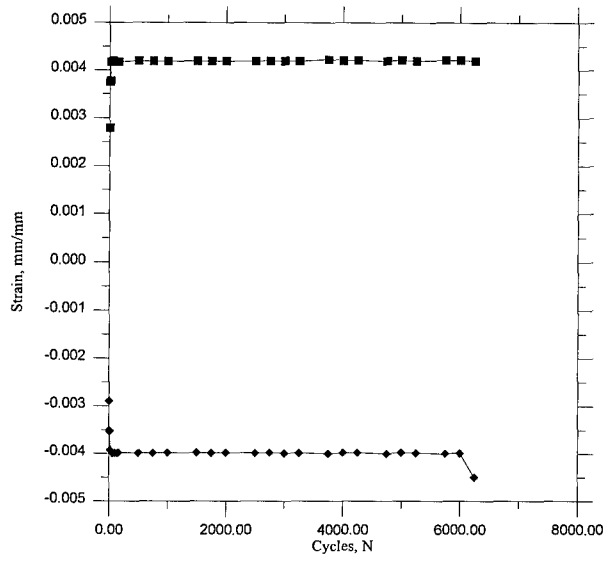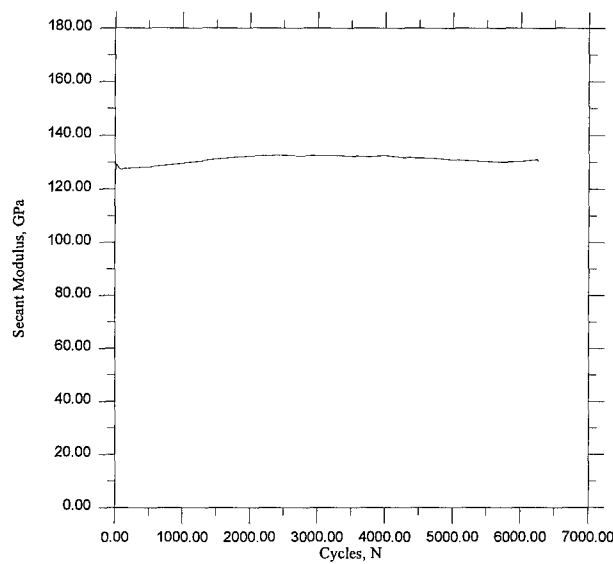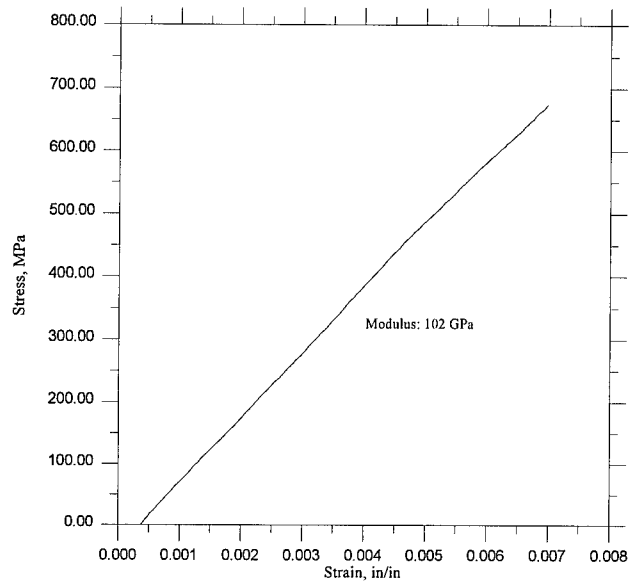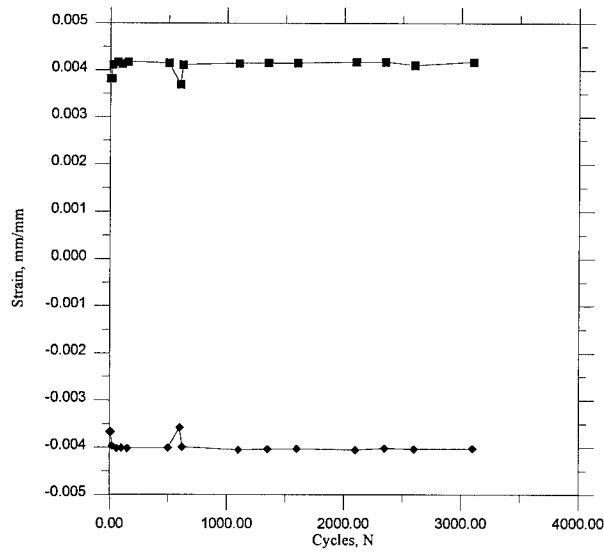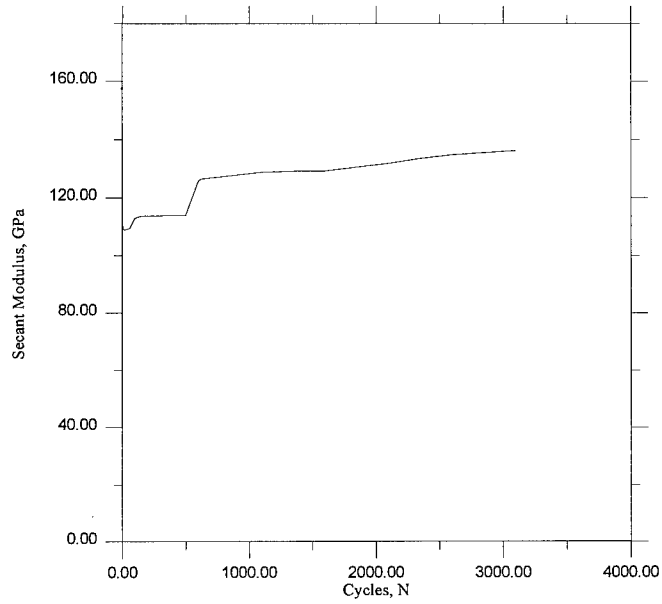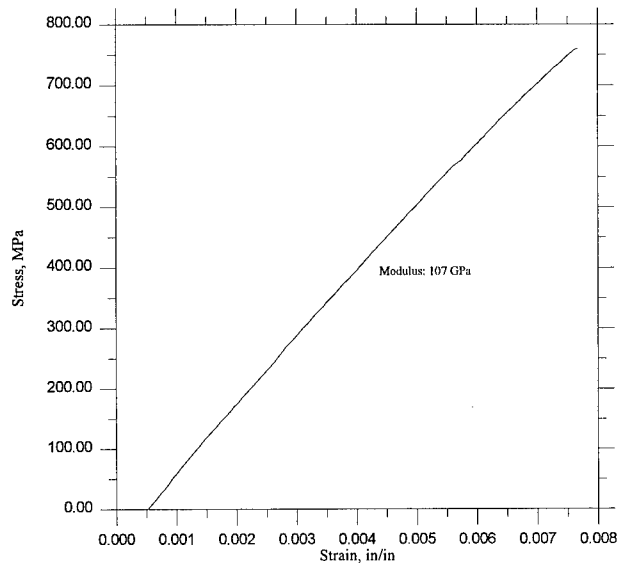Figure 70. Monotonic Test to Failure, 0.4% Maximum Strain, 25% Expected Life

Bibliography

[1] Boyum, E. A. *Investigation of Tension-Compression Fatigue Behavior of a Cross-Ply Metal Matrix Composite at Room and Elevated Temperatures*. MS thesis, AFIT/GAE/ENY/93D-6. School of Engineering, Air Force Institute of Technology, Wright-Patterson AFB, OH, December 1993.

[2] Boyum, Elizabeth A. and S. Mall. "Fatigue Behavior of a Cross-Ply Titanium Matrix Composite under Tension-Tension and Tension-Compression Cycling," *Materials Science and Engineering*, *Vol A200*, 1–11, 1995.

[3] Calcaterra, J.R., S. Mall A. Ruiz. "Differences in the Residual Strength Degradation of SCS-6/Ti-15-3 Based on Laminate Orientation, R-Ratio, and Control Mode," 1997. To be Submitted for Publication (1997).

[4] Chiou, Sen-Tzer. *Residual Strength After Fatigue on Uniderectional and Cross-Ply Metal Matrix Composite at Elevated Temperature*. MS Thesis, AFIT/GAE/ENY/96J-2. School of Engineering, Air Force Institute of Technology, Wright-Patterson AFB, OH, June 1996.

[5] Coughlan, Sean. *Fiber Volume Fraction Effects on Fatigue Response of a SCS-6/Ti-15-3 Metal Matrix Composite at Elevated Temperature*. MS thesis, Air Force Institute of Technology, Wright-Patterson AFB, OH, June 1997.

[6] Covey, S.J., B.A. Lerch and N. Jayaraman. "Fiber Volume Fraction Effects on Fatigue Crack Growth in SiC/Ti-15-3 Composite," *Materials Science and Engineering*, *Vol. A200*, 68–77, 1995.

[7] Dennis, Leon B. *Fatigue Behaviour of a Cross-Ply Metal Matrix Composite at Elevated Temperature Under Strain Controlled Mode*. MS thesis, AFIT/GAE/ENY/94D-7. School of Engineering, Air Force Institute of Technology, Wrigth-Patterson AFB, OH, 1994.

[8] Gabb, T.P., J. Gayda B.A. Lerch and G.R. Halford. "The Effect of Matrix Mechanical Properties on [0]8 SiC/Ti Composite Fatigue Resistance," *Scripta Metalurgica et Materiala*, *Vol 25*, 2879–2884, 1991.

[9] Gayda, J.and T.P. Gabb. "The Effect of Fiber Content on the Fatigue Life of SCS6/Ti-15-3 Composite," *Scripta Metalurgica et Materiala*, *Vol. 30*, 469–474, 1994.

[10] Jackson, Sean C. *Stress/Strain Ratio Effects on Fatigue Response of a SCS-6/Ti-15-3 Metal Matrix Composite at Elevated Temperature*. MS thesis, AFIT/GAE/ENY/95D-14, School of Engineering, Air Force Institute of Technology, Wright-Patterson, AFB, OH, December 1994.

[11] Johnson, W. S., S. J. Lubowinski Alton L. Highsmith. "Mechanical Characterization of Unnotched SCS6/Ti-15-3 Metal Matrix Composites at Room Temperature," *American Society for Testing and Materials,*, 193–218, 1990.

[12] Kraabel, D. L. *Investigation of Tension-Compression Fatigue Behavior of a Unidirectional Metal Matrix Composite at Elevated Temperature*. MS thesis, AFIT/GAE/ENY/94D. School of Engineering, Air Force Institute of Technology, Wrigth-Patterson AFB, OH, December 1994.

[13] Lee, Sang-Myung. *Residual Strength and Fatigue Characterization of SCS-6/Ti-6-4*. MS thesis, AFIT/GAE/ENY/96D-17. Air Force Institute of Technology, Wrigth-Patterson AFB, OH, 1996.

[14] Lerch, Bradley A. and James F. Saltsman. "Tensile Deformation Damage in SiC Reinforced Ti-15V-3Cr-3Al-3Sn," *NASA Technical Memorandum 103620,*, 1–20, April, 1991.

[15] Majundar, B. S. and Newas G. M. "Inelastic Deformation of Metal Matrix Composites: Plasticity and Damage Mechanisms," *Philosophical Magazine*, *Vol. 66, No.2,* 187–212, 1992.

[16] Mallick, P.K. *Fiber-Reinforced Composites* (Second Edition). 270 Madison Avenue, New York, New York 10016: Marcel Dekker, Inc., 1993.

[17] Newas, G. M. and B. S. Majumdar. "Deformation and Failure Mechanism in Metal Matrix Composites," *ASME*, *AD-Vol. 22/AMD-Vol. 122,* 55–65, 1991.

[18] Newas, Golam M. and Bhaskar S. Majumdar. *Inelastic Deformation Mechanisms in SCS-6/Ti 15-3 MMC Lamina Under Compression*. Technical Report NASA Contractor Report 191170, Columbus, Ohio: Battelle Memorial Institute, September 1993.

[19] Nicholas, T., S.M. Russ R.W. Neu and N. Schehl. "Life Prediction of a [0/90] Metal Matrix Composite Under Isothermal and Thermomechanical Fatigue," *Composites Science and Technology*, *Vol. 52,* 27–36, March, 1994.

[20] Nicholas, T. and J. Ahmad. "Modeling Fiber Breakage in a Metal-Matrix Composite," *Composites Science and Technology*, *Vol. 52,* 29–38, 1994.

[21] Pittman, Robert. *Frequency Effects on Fatigue Behavior of a Unidirectional Metal Matrix Composite at Elevated Temperature*. MS thesis, AFIT/GAE/ENY/95D. School of Engineering, Air Force Institute of Technology, Wrigth-Patterson, AFB, OH, December, 1995.

[22] Pollock, William D. and W. Steven Johnson. "Characterization of Unnotched SCS-6/Ti-15-3 Metal Matrix Composites at 650 C," *Composite Materials: Testing and Design*, *Vol 10,* 175–191, 1992].

[23] Portner, Barry D. *Investigation of Fatigue Damage Mechanism in a Metal Matrix Composite under Elevated Temperature*. MS Thesis, AFIT/GAE/ENY/90D-20. Air Force Institute of Technology, Wright-Patterson AFB, OH, December 1990.

[24] Sanders, Brian and Shankar Mall. "Isothermal Fatigue Behavior of a Titanium Matrix Composite under a Hybrid Strain-Controlled Loading Condition," *Materials Science and Engineering*, *Vol. A200,* 130–139, 1995.

[25] Talreja, Ramesh. "A Conceptual Framework for Interpretation of MMC Fatigue," *Material Science and Engineering*, *Vol A200,* 21–28, 1995.

[26] Taya, Minoru and Richard J. Arsenault. *Metal Matrix Composites: Thermomechanical Behavior*. Oxford: Pergamon Press, 1989.

Vita

Captain Alvin Ruiz, US Army, ██████████████████████████████████

██ He graduated from CONSA High School in Santo Domingo, Dominican Republic, in 1979 and, in 1980, joined the US Army as an enlisted soldier. Upon completion of his three years enlistment, he attended the University of Bridgeport, Bridgeport, Connecticut were he graduated with a Bachelor of Science in Mechanical Engineering and received a commission as a Second Lieutenant in the United States Army. He served as an Infantry Officer in the Republic of Panama and later on as a Company Commander in the 154th Signal Battalion. Following his assignment in Panama he entered the Air Force Institute of Technology in October 1995.

REPORT DOCUMENTATION PAGE

Form Approved
OMB No. 0704-0188

1. AGENCY USE ONLY (Leave blank)	2. REPORT DATE June 1997	3. REPORT TYPE AND DATES COVERED Master Thesis

4. TITLE AND SUBTITLE
Residual Strength After Fatigue of a Cross-Ply Metal Matrix
Composite at Elevated Temperature

5. FUNDING NUMBERS

6. AUTHOR(S)
Alvin Ruiz, CPT, US Army

7. PERFORMING ORGANIZATION NAME(S) AND ADDRESS(ES)
Air Force Institute of Technology, WPAFB OH 45433-6583

8. PERFORMING ORGANIZATION REPORT NUMBER
AFIT/GAE/ENY/97J-1

9. SPONSORING / MONITORING AGENCY NAME(S) AND ADDRESS(ES)
AFOSR/NA
Bolling AFB DC 20332

10. SPONSORING / MONITORING AGENCY REPORT NUMBER

11. SUPPLEMENTARY NOTES

12a. DISTRIBUTION / AVAILABILITY STATEMENT
Approved for public release; distribution unlimited

12b. DISTRIBUTION CODE
A

13. ABSTRACT (Maximum 200 words)

The objective of this study was to investigate the residual strength of a cross-ply, SCS-6/Ti-15-3, metal matrix composite (MMC) at elevated temperature (427°C) when exposed to fatigue loading. Several specimens were subjected to a strain-controlled, fully reversed loading (R= -1), at various strain levels. The specimens were fatigued up to a portion of their life expectancy and then loaded to failure. Stress and strain data obtained during the test provided useful information for the macro-mechanical behavior of the material. It was determined that the residual strength was directly related to the amount of damage present in the matrix, meanwhile, the amount of matrix damage was dependent on the number of cycles and strain level the specimen had been exposed to. It was also observed that the residual strength under the strain controlled mode degraded more consistently than its counterpart under load controlled mode. This variation, however, may be due to the frequency and R-ratio differences between the two loading modes. The comparison of the residual strength degradation of the cross-ply vs. unidirectional laminates reflected a significant difference due to ply orientation. The unidirectional composite exhibited much less residual strength degradation due to the absence of the crack initiation action attributed to the 90° plies in the cross-ply.

14. SUBJECT TERMS
Residual Strength, Metal Matrix Composite, Fatigue Loading
Cross-ply, SCS-6/Ti-15-3

15. NUMBER OF PAGES
106

16. PRICE CODE

17. SECURITY CLASSIFICATION OF REPORT Unclassified	18. SECURITY CLASSIFICATION OF THIS PAGE Unclassified	19. SECURITY CLASSIFICATION OF ABSTRACT Unclassified	20. LIMITATION OF ABSTRACT UL

GENERAL INSTRUCTIONS FOR COMPLETING SF 298

The Report Documentation Page (RDP) is used in announcing and cataloging reports. It is important that this information be consistent with the rest of the report, particularly the cover and title page. Instructions for filling in each block of the form follow. It is important to *stay within the lines* to meet *optical scanning requirements.*

Block 1. Agency Use Only *(Leave blank)*.

Block 2. Report Date. Full publication date including day, month, and year, if available (e.g. 1 Jan 88). Must cite at least the year.

Block 3. Type of Report and Dates Covered. State whether report is interim, final, etc. If applicable, enter inclusive report dates (e.g. 10 Jun 87 - 30 Jun 88).

Block 4. Title and Subtitle. A title is taken from the part of the report that provides the most meaningful and complete information. When a report is prepared in more than one volume, repeat the primary title, add volume number, and include subtitle for the specific volume. On classified documents enter the title classification in parentheses.

Block 5. Funding Numbers. To include contract and grant numbers; may include program element number(s), project number(s), task number(s), and work unit number(s). Use the following labels:

C	-	Contract	PR	-	Project
G	-	Grant	TA	-	Task
PE	-	Program Element	WU	-	Work Unit Accession No.

Block 6. Author(s). Name(s) of person(s) responsible for writing the report, performing the research, or credited with the content of the report. If editor or compiler, this should follow the name(s).

Block 7. Performing Organization Name(s) and Address(es). Self-explanatory.

Block 8. Performing Organization Report Number. Enter the unique alphanumeric report number(s) assigned by the organization performing the report.

Block 9. Sponsoring/Monitoring Agency Name(s) and Address(es). Self-explanatory.

Block 10. Sponsoring/Monitoring Agency Report Number. *(If known)*

Block 11. Supplementary Notes. Enter information not included elsewhere such as: Prepared in cooperation with...; Trans. of...; To be published in.... When a report is revised, include a statement whether the new report supersedes or supplements the older report.

Block 12a. Distribution/Availability Statement. Denotes public availability or limitations. Cite any availability to the public. Enter additional limitations or special markings in all capitals (e.g. NOFORN, REL, ITAR).

DOD - See DoDD 5230.24, "Distribution Statements on Technical Documents."
DOE - See authorities.
NASA - See Handbook NHB 2200.2.
NTIS - Leave blank.

Block 12b. Distribution Code.

DOD - Leave blank.
DOE - Enter DOE distribution categories from the Standard Distribution for Unclassified Scientific and Technical Reports.
NASA - Leave blank.
NTIS - Leave blank.

Block 13. Abstract. Include a brief *(Maximum 200 words)* factual summary of the most significant information contained in the report.

Block 14. Subject Terms. Keywords or phrases identifying major subjects in the report.

Block 15. Number of Pages. Enter the total number of pages.

Block 16. Price Code. Enter appropriate price code *(NTIS only)*.

Blocks 17. - 19. Security Classifications. Self-explanatory. Enter U.S. Security Classification in accordance with U.S. Security Regulations (i.e., UNCLASSIFIED). If form contains classified information, stamp classification on the top and bottom of the page.

Block 20. Limitation of Abstract. This block must be completed to assign a limitation to the abstract. Enter either UL (unlimited) or SAR (same as report). An entry in this block is necessary if the abstract is to be limited. If blank, the abstract is assumed to be unlimited.